Hydrol. Earth Syst. Sci. Discuss., 10, 1127–1183, 2013
www.hydrol-earth-syst-sci-discuss.net/10/1127/2013/
doi:10.5194/hessd-10-1127-2013

Hydrology and Earth System Sciences Discussions

Three perceptions of the evapotranspiration landscape: comparing spatial patterns from a distributed hydrological model, remotely sensed surface temperatures, and sub-basin water balances

T. Conradt[1], F. Wechsung[1], and A. Bronstert[2]

[1]Potsdam Institute for Climate Impact Research, Potsdam, Germany
[2]Institute of Earth and Environmental Science, University of Potsdam, Potsdam, Germany

Received: 8 January 2013 – Accepted: 13 January 2013 – Published: 24 January 2013

Correspondence to: T. Conradt (conradt@pik-potsdam.de)

Published by Copernicus Publications on behalf of the European Geosciences Union.

Abstract

A problem encountered by many distributed hydrological modelling studies is high simulation errors at interior gauges when the model is only globally calibrated at the outlet. We simulated river runoff in the Elbe River basin in Central Europe (148 268 km^2) with the semi-distributed eco-hydrological model SWIM. While global parameter optimisation led to Nash–Sutcliffe efficiencies of 0.9 at the main outlet gauge, comparisons with measured runoff series at interior points revealed large deviations. Therefore, we compared three different stategies for deriving sub-basin evapotranspiration: (1) modelled by SWIM without any spatial calibration, (2) derived from remotely sensed surface temperatures, and (3) calculated from long-term precipitation and discharge data. The results show certain consistencies between the modelled and the remote sensing based evapotranspiration rates, but there seems to be no correlation between remote sensing and water balance based estimations. Subsequent analyses for single sub-basins identify input weather data and systematic error amplification in inter-gauge discharge calculations as sources of uncertainty. Further probable causes for epistemic uncertainties could be pinpointed. The results encourage careful utilisation of different data sources for calibration and validation procedures in distributed hydrological modelling.

1 Introduction

1.1 Improving spatial representativeness of distributed models

A distributed hydrological model which accurately simulates discharges at the basin outlet while producing poor results at interior points seems to be a paradox. But this feature has been shown by many studies on distributed modelling where inner point discharges were evaluated. Examples for larger simulation errors within the model domain give Andersen et al. (2001), Güntner (2002), Ajami et al. (2004), Ivanov et al. (2004) (suggesting a synthesis of modelling with remote sensing data to realise “the

HESSD
10, 1127–1183, 2013

true value of the distributed approach"!), Mo et al. (2006), Moussa et al. (2007), Feyen et al. (2008), or Merz et al. (2009). Bergström and Graham (1998) and Das et al. (2008) report better model performances with increasing basin size for (semi-) lumped approaches, too. Pokhrel and Gupta (2010) and Pechlivanidis et al. (2010) tried parameter-sparse approaches for multi-site calibration but achieved generally poor model performances at interior points. Finally, respective results obtained from numerous models in the first phase of the "Distributed Model Intercomparison Project" (Reed et al., 2004) gave rise to adding more stream gauges at interior points for the second project phase (Smith et al., 2012a) which confirmed the observed trend of model fidelity increasing with basin size (Smith et al., 2012b).

Yet another example from the Elbe River basin in Central Europe (148 268 km^2) gave reason to this study: for estimating water-related climate change impacts, the semi-distributed eco-hydrological model SWIM had been applied to project natural water discharges under scenario conditions (Conradt et al., 2012b, 2013a). Single global calibration by measured discharges at the basin outlet appeared to be insufficient: comparing the simulated discharges from higher-order tributaries by respective gauge data often revealed grave deviations in water volume. Figure 1 shows the relative volume errors decreasing with increasing sub-basin area. Other comparisons showed poor model performance in simulating peak or low flow phases for some sub-areas of the basin. Nevertheless, a Nash–Sutcliffe efficiency of 0.9 had been achieved for long-term series of daily discharge at the main outlet gauge Neu Darchau.

While studies devoted to spatial representativeness of distributed models have not received much attention yet, the related general modelling problem "to be right for the wrong reasons" (cf. Klemeš, 1982) has incited a broad and still ongoing discussion among hydrologists about the representativeness of their models in general (e.g. Klemeš, 1986; Beven, 1989, 1996; Grayson et al., 1992; Blöschl, 2001; Andréassian et al., 2007, 2012; Sivakumar, 2008, to name just a few out of dozens of contributions).

Spatial calibration might minimise sub-catchment uncertainties through increasing site-specific representativeness of the model. In conjunction with distributed

HESSD
10, 1127–1183, 2013

hydrological modelling, spatial calibration usually means individual multi-site calibration (Santhi et al., 2008; Zhang et al., 2008). This study uses the term in the same line; it should not be confused with either multi-objective calibrations of global model parameters based on sub-catchment spatio-temporal data (e.g. Zhang et al., 2010; Xie et al., 2012) or data assimilation of which Schuurmans et al. (2011) give an example with weighted averages from satellite-derived and modelled evapotranspiration (ET).

Spatial calibration in the narrower sense provides specific research opportunities. Seibert et al. (2000) found optimal subcatchment modelling results for individual parameter settings, while Khakbaz et al. (2012) explain their opposite finding by a homogeneous basin. In any case, regional patterns of optimised sub-basin parameters as observed by DeMarchi et al. (2011) or Conradt et al. (2012a) add credibility to the approach and can be object of further investigation. Partial spatial calibration is also possible: Bronstert et al. (2007) concentrated calibration efforts on some few selected small sub-catchments and on a number of main stream gauges of the Rhine.

Pokhrel and Gupta (2011) argue that enhancements of spatial model representativeness are not necessarily seen in the outlet hydrograph. But they agree with other researchers that incorporating additional site-specific information in a distributed hydrological model increases its robustness (Stisen et al., 2011). Especially remote sensing data are valued as useful complement to station based time series (Finger et al., 2011; Liu et al., 2012).

In our case of semi-distributed eco-hydrological modelling of the Elbe River basin (Conradt et al., 2012a,b), sub-basin discharges were fitted to (management corrected) gauge observations by individual evapotranspiration corrections. Having calibrated the model globally beforehand, most sub-basin ET adjustment factors differed significantly from one. High and low values were spatially clustered, but no functional relationship to certain land use classes or soil types could be identified. An independent mapping of the spatial ET pattern by means of remote sensing could probaby explain these observations and help to identify probable error sources.

HESSD
10, 1127–1183, 2013

1.2 Hydrological modelling and remote sensing

The idea of integrating remote sensing into hydrological modelling is relatively old (e.g. Klemeš, 1983, 1988; Schultz, 1987, 1988), and despite many systematic and practical problems (cf. Kite and Pietroniro, 1996; Beven, 1996, 2001) a lot of modellers continued working with remotely sensed data in recent years. As satellite data availability has much been increased within the last decade, current research is finally measuring up with many expectations of the 1980s (Nagler, 2011). For example, an operational, multiple-source data assimilation system integrating remote sensing information is currently being put into service in Australia (van Dijk and Renzullo, 2011; Glenn et al., 2011).

We use remotely sensed land surface temperatures to map the ET pattern in the Elbe River basin. Recent studies that also make use of thermal and optical sensors range from "classical" rainfall-runoff modelling with remotely sensed pattern comparison (like our contribution) to integrated data assimilation systems. Examples of the former are Boegh et al. (2004) for 10 km^2 of agricultural landscape in Denmark or Vinukollu et al. (2012) with a global ET pattern comparison. A substantial contribution is also Schuurmans et al. (2011) who first compare and then assimilate the modelled and remotely sensed actual ET patterns of an area of 70 km^2 in the middle of the Netherlands; observed differences between the two data sources remain partly unexplained, however.

Despite the fact that remote sensing does not directly provide measurements that a hydrological model could be calibrated to, the idea of using the additional spatial information for improving distributed models seems to be an elegant way between the extremes of validation only and direct data assimilation.

Immerzeel and Droogers (2008), for example, applied the SWAT model to the Upper Bhima catchment in southern India (45 678 km^2) and adjusted the monthly evapotranspiration for each sub-basin to the ET_a-estimates of the SEBAL-algorithm (Bastiaanssen et al., 1998a,b) applied to thermal imagery from the MODIS satellite. Singh et al. (2010) and Jhorar et al. (2011) used remotely sensed ET rates for improving

HESSD
10, 1127–1183, 2013

agro-hydrological models on irrigated plots. And Githui et al. (2012) demonstrated a multi-objective and spatial calibration of a semi-distributed model using data from two runoff gauges and remotely sensed ET for 59 sub-basins of the 600 km^2 Barr Creek catchment in northern Victoria, Australia.

1.3 Objectives of this study

Originally, our intention was to present an alternative spatial calibration of our Elbe River basin model by means of remote sensing. But we will make a more fundamental assessment by comparing annual evapotranspiration patterns in space derived by:

1. the semi-distributed eco-hydrological model SWIM,
2. an approach based on remotely sensed land surface temperatures, and
3. the water balance method.

The objectives are to show the feasability of our remote sensing approach, to evaluate the correspondencies and differences between the results of all three methods, and to find reasonable explanations for systematic or individual sub-basin deviations. The potential of the remote sensing approach for alternative spatial calibration of the hydrological model may be fathomed as well.

1.4 The Elbe River basin

Before we present the three methods in detail, the research domain shall be introduced. The Elbe River basin, located in central Europe covers 148 268 km^2 (FGG Elbe), thereof approximately one third within the Czech Republic and two thirds within Germany; less than 1 % belong to Austria and Poland. Figure 2 provides two maps of the basin.

The model domain was restricted to 134 890 km^2, including the drainage area of the main outlet gauge Neu Darchau (131 950 km^2). The lower part of the stream is influenced by tide, which renders continuous discharge measurements impossible.

Approximately 50 % of the area are lowlands below 200 m a.m.s.l. This landscape dominates the north of the basin. Formed by the last glaciations, it is characterised by sandy plateaus with loam-covered riparian zones and wetlands in between. Due to the low slopes, sandy soils, and comparably low-intensity rainfall, the hydrological behaviour is governed by groundwater dynamics. Major land uses are grassland, forestry, and agriculture, often on poor soils.

The higher elevated regions can be divided up into hilly mountain forelands (32 %, 200–500 m a.m.s.l.) and mountaineous areas (18 %, above 500 m a.m.s.l.). The hilly mountain forelands are covered by loamy–silty substrates and loess areas of highest field capacities. These productive soils are mainly used for agriculture. The mountaineous areas have relatively poor soils, typically thin cambisols from weathered rock sediments. Their major land use are coniferous forests. The highest point of the basin is marked by the mountain Sněžka (Czech) or Śnieżka (Polish) on the border between the Czech Republic and Poland. It reaches an altitude of 1602 m a.m.s.l.

Climatically, the Elbe River basin is located at the transition of the maritime temperate zone towards continental climate. Precipitation shows a rather uniform intra-annual distribution. The long-term mean is 702 mm a^{-1}, and the average discharge at the river mouth of 861 $m^3 s^{-1}$ equals 183 mm a^{-1}, which means an average evapotranspiration of 519 mm a^{-1} (FGG Elbe, and own calculations). The spatial distribution of precipitation depends strongly on topography: near Magdeburg, in the lee of the Harz Mountains, less than 500 mm a^{-1} are measured, while more than 1200 mm a^{-1} can be observed within the mountaineous regions. Evapotranspiration follows a distinct annual cycle. Negligible in winter, local ET rates reach up to 7 mm d^{-1} in summertime.

There are huge lignite open cast mining areas in the sub-basins of the rivers Spree, Schwarze Elster, and Weiße Elster. These are hydrologically important: a groundwater deficit of 13×10^9 m^3 had been created by draining (Grünewald, 2001), and ongoing recultivation activities shall produce over 200 km^2 of new water surfaces. Besides direct effects on river discharge, the landscape alterations affect local hydrometeorology (Conradt et al., 2007).

HESSD
10, 1127–1183, 2013

The spatial pattern of climatic inputs and a multitude of different landforms, soil characteristics, and land uses within the Elbe River basin make it an interesting large-scale domain for distributed hydrological modelling. Examples are the contributions by Krysanova et al. (1999), who observed unsatisfactory model performance in the lowlands (in particular the Havel River) where the runoff regime is dominated by river–groundwater interactions and the related transpiration fluxes in the riparian areas, or Krause and Bronstert (2007) who focused their investigation on these processes.

In contrast to the similar studies of Immerzeel and Droogers (2008) and Githui et al. (2012), records from 133 gauging stations within the Elbe area could be utilized for comparison. As the water balance method requires long-term observations, mean discharges of 1961–1990 were used where available. Some gauge data were restricted to shorter periods that fell into this time-span. Comparisons with model results were always made for matching periods, this applies accordingly for the remote sensing estimations.

2 Methods

2.1 Evapotranspiration modelling

2.1.1 General model structure

The semi-distributed eco-hydrological model SWIM (Krysanova et al., 1998, 2000) is a variant of the well-known SWAT (Arnold et al., 1993, 1998; Srinivasan et al., 1998; Gassman et al., 2007). Semi-distributed means that the model domain is not represented in gridded manner (fully distributed) but by landscape patches with uniform hydrological behaviour, the so-called hydrotopes. For this study, the model domain had initially been divided up into 2278 sub-basins. In the following, they shall be addressed as “model sub-basins” to distinguish them from (gauged) sub-basins in general. 133 calibration sub-basins are gauged aggregations of these model sub-basins.

The hydrotopes are sub-units of these model sub-basins, defined by an intersection of soil and land use maps so that each hydrotope is a unique combination of sub-basin, soil type and land use.

For each hydrotope, vegetation growth and water and nutrient fluxes between various storages are modelled. This comprises, e.g. water seepage and capillary rise between soil layers, water and nutrient stress for plants, or evapotranspiration. Discharge components are accumulated and routed through the sub-basin structure by the Muskingum approach. The model works on a daily timestep.

Daily climate input was provided by measurements of 853 climate stations, 352 thereof fully instrumented, and 501 rain gauges. Input variables were precipitation, global radiation, air humidity, and maximum, minimum, and mean air temperature. These data were interpolated to the model sub-basins with inverse-distance weighting. Elevation dependencies were considered individually for each variable: when a linear regression on elevation yielded a coefficient of determination exceeded of at least 0.4, only the residuals were interpolated and the trend component added afterwards.

2.1.2 The evapotranspiration calculus

A modified Turc–Ivanov approach (Richter, 1984; Wendling and Schellin, 1986; DVWK) which is applicable without wind speed data was used for calculating reference evapotranspiration. The original formula by Turc (1961) is replaced by another approach originally proposed by Ivanov (1954) when the daily average temperature T remains below 5 °C:

$$\mathrm{ET_p} = \begin{cases} 0.0031 \cdot \Omega \cdot (R_\mathrm{n} + 209.4) \cdot \left(\frac{T}{T+15}\right) & \text{for} \quad T \geq 5 \\ 0.000036 \cdot (T+25)^2 \cdot (100 - \mathrm{rF}) & \text{for} \quad T < 5 \end{cases} \tag{1}$$

This combined equation yields daily potential or reference evapotranspiration $\mathrm{ET_p}$ in mm from average temperature T in °C, net radiation R_n in $\mathrm{J\,cm^{-2}}$, and relative humidity rF in %. The dimensionless factor Ω varies monthly between 0.7 for December and January and 1.25 for May.

HESSD
10, 1127–1183, 2013

According to ATV-DVWK, the reference ET_p values from Eq. 1 were modified by land use specific factors ranging between 0.9 for cropland and 1.3 for water surfaces.

Daily actual evapotranspiration ET_a is then calculated for each hydrotope as sum of soil evaporation ES and plant transpiration EP with an approach similar to that of Ritchie (1972).

Plant transpiration is calculated from the reference ET_p depending on the leaf area index LAI:

$$EP_0 = \begin{cases} \frac{ET_p \cdot LAI}{3} & \text{for } 0 \leq LAI \leq 3 \\ ET_p & \text{for } \quad LAI > 3 \end{cases} \tag{2}$$

This preliminary value EP_0 is reduced to EP according to the plant actual plant water use which is calculated for each soil layer separately according to the approach of Williams and Hann (1978): a potential water use WUP_i for layer i is estimated with the equation

$$WUP_i = \frac{EP_0}{1 - \exp(RDP)} \cdot \left[1 - \exp\left(-\frac{RDP \cdot RZD_i}{RD}\right)\right] \tag{3}$$

where RDP refers to a "rate depth parameter", RZD_i means "root zone depth parameter of layer i", and RD is the fraction of the root zone that contains roots. The actual water use from that layer WU_i depends on the ratio of available soil water SW_i to the field capacity FC_i:

$$WU_i = \begin{cases} WUP_i \cdot \frac{SW_i}{0.25 \cdot FC_i} & \text{for } SW_i \leq 0.25\,FC_i \\ WUP_i & \text{for } SW_i > 0.25\,FC_i \end{cases} \tag{4}$$

Soil evaporation is treated in similar steps; starting with potential soil evaporation which depends on LAI, the value is reduced according to the extent of dry periods and available water in the top 30 cm of the soil.

HESSD
10, 1127–1183, 2013

The amount of evapotranspirated water is subtracted from the soil layer storages and accordingly reduces percolation and subsurface and ground water runoff and, subsequently, the accumulated discharge.

2.2 Estimating ET from land surface temperatures

Evapotranspiration can not be measured directly from space, but several methods exist to estimate ET values by means of remote sensing. One common approach is based on surface temperature, which can be inferred from thermal radiation and is partly governed by energy partitioning into sensible and latent heat. Most studies following this approach aimed at estimating evapotranspiration more or less solely from remotely sensored data; their comparisons with ground measurements show correlations, but typically high noise levels (Moran et al., 1994; Kite and Droogers, 2000; Garatuza-Payan et al., 2001; Jiang and Islam, 2001; Jacobs et al., 2004; Patel et al., 2006; Wloczyk, 2007; Hoedjes et al., 2008; Galleguillos et al., 2011).

Bastiaanssen et al. (1998a,b) invented the SEBAL-algorithm to account for many error sources by taking the coolest ("wet") and the warmest ("dry") pixel of a scan as calibration basis. This approach may well be the most popular in counts of applications, derived variants and further developments, e.g. Gómez et al. (2005); Verstraeten et al. (2005); Koloskov et al. (2007); Stisen et al. (2008); Long and Singh (2010); Schuurmans et al. (2011).

Many problems of ET estimation from thermal radiances – which also contribute to the challenges of this study – can be explained from a closer look at the relationships between energy and water fluxes. The general energy balance for any surface spot on the Earth reads:

$$R_n + G + S = \lambda ET + H \quad (5)$$

On the left hand side, the energy inputs net radiation R_n, ground heat flux G and heat advection S are summed up. They equal the outgoing fluxes on the right hand side: latent heat by evapotranspiration λET and sensible heat H. Net radiation is principally the driving force for evapotranspiration. The other input terms, G and S, may be neglected for 24 h and a fortiori for annual integrations, but both net radiation and Bowen ratio (of sensible to latent heat) have to be determined.

2.2.1 Determining net radiation

Net radiation is the sum of all radiation components at the ground:

$$R_n = (1-\alpha)\cdot R_{sg} + R_{la}\downarrow - R_{le}\uparrow \tag{6}$$

In detail, R_n consists of that part of the incoming short-wave global radiation R_{sg} which is not reflected at the surface (therefore α, the land cover dependent albedo), and the long-wave components: surface radiation R_{le} towards the sky (therefore negative) and atmospheric back-radiation R_{la}. While αR_{sg} and R_{le} may be quite directly measured by a remote sensor (only corrected for atmospheric extinction), assumptions or ground measurements have to be made for determining R_{la} and the total global radiation R_{sg}, or R_{la} and α, respectively.

The relationship between thermal radiances and actual surface temperature provides additional room for errors, because the Stefan-Boltzmann law $R = \varepsilon\cdot\sigma\cdot T^4$ contains the emission coefficient ε which depends on the radiant material. T denotes the temperature in K and σ is the Stefan-Boltzmann constant of 5.67 $\mathrm{W\,m^{-2}\,K^{-4}}$. Both R_{la} and R_{le} can be expressed in terms of specific ε and T values:

$$R_{la} = \varepsilon_a\cdot\sigma\cdot T_a^4 \tag{7}$$

$$R_{le} = \varepsilon_e\cdot\sigma\cdot T_e^4 \tag{8}$$

While ε_e varies only within a small range around 0.95 for natural surfaces (Albertz, 1991), the assumption of a single temperature T_a for the atmosphere is a common simplification, and air temperatures can hardly be measured remotely. The SEBAL method mentioned above helps to circumnavigate the latter problem. For this study, conventionally ground-measured temperature and radiation data are utilized.

HESSD
10, 1127–1183, 2013

Net radiation is routinely derived by SWIM from standard input data containing daily values of global radiation R_{sg}, air temperature T_a, and relative humidity rF. The formulæ in the applied SWIM version generally follow the recommendations of DVWK. Equation (6) is fed with albedo depending on vegetation density and eventual snow coverage:

$$\alpha = \begin{cases} 0.23\,(1-\nu) + 0.15\,\nu & \text{for} \leq 5\,\text{mm water equivalent} \\ 0.6 & \text{for thicker snow cover} \end{cases} \tag{9}$$

$$\nu = \exp[-5 \cdot 10^{-5} \cdot (d_\nu + 0.1)] \tag{10}$$

with d_ν being the biomass density in $\text{kg}\,\text{ha}^{-1}$ dynamically calculated by the crop and vegetation growth routines. Furthermore, Eqs. (7) and (8) are merged to a net emittance with the effective emission coefficient ε' and a cloud cover factor ϖ:

$$R_{la} - R_{le} = \sigma \cdot \varepsilon' \cdot \varpi \cdot T_a^4 \tag{11}$$

using the approximations of Brunt (1932) based on vapour pressure e

$$\varepsilon' = 0.34 - 0.044 \cdot \sqrt{e} \tag{12}$$

which, despite its age, seems to perform better than more recently developed alternatives (cf. Bilbao and Miguel, 2007; Choi et al., 2008), and Wright and Jensen (1972) with coefficients by Doorenbos and Pruitt (1977)

$$\varpi = 0.1 + 0.9 \cdot \frac{R_{sg}}{R_{max}} \tag{13}$$

The vapour pressure e is calculated from T_a and rF according to DVWK, and R_{max} is the theoretically possible clear-sky radiation on the given day at the mean latitude of the model domain.

HESSD
10, 1127–1183, 2013

2.2.2 Determining the Bowen ratio

Equation (5) shifted about neglecting G and S and divided by $\lambda = \varrho_w \cdot r_v$, which is the energy needed to evaporate one volume unit of water (water density ϱ_w times steam heat r_v), delivers ET, when both R_n and H are known:

$$\mathrm{ET} = \frac{1}{\lambda}(R_n - H) \tag{14}$$

The calculation of net radiation has been discussed above. The question remains, how much of R_n is transformed into sensible heat and what remains for evapotranspiration, i. e., the Bowen ratio (Bowen, 1926a,b; Lewis, 1995) has to be determined.

The sensible heat flux H is driven by the vertical temperature gradient $\frac{\partial T}{\partial z}$. In practice, this gradient is represented by the temperature difference $\Delta T = T_s - T_a$ between the soil or plant canopy surface temperature T_s and the 2 m air temperature T_a. The sensible heat flux can then be formulated either via an exchange coefficient C or an aerodynamic resistance for heat r_{ah}:

$$H = \Delta T \cdot c_p C = \Delta T \cdot \frac{\varrho_a c_p}{r_{ah}} \tag{15}$$

In this equation, c_p means the sprecific heat content of the air and ϱ_a its density. Aerodynamic resistance (viz. the exchange coefficient) depends on atmospheric stability, wind velocity u (at a reference height z) and geometric surface characterisics. The latter can be parameterised by zero plane displacement height d and roughness lengths for sensible heat z_{0h} and momentum z_{0m}. According to the Monin–Obukhov theory of surface layer similarity (Monin and Obukhov, 1954), r_{ah} is then given by

$$r_{ah} = \frac{\left[\ln\left(\frac{z-d}{z_{0h}}\right) - \psi_{sh}\right] \cdot \left[\ln\left(\frac{z-d}{z_{0m}}\right) - \psi_{sm}\right]}{k^2 \cdot u(z)} \tag{16}$$

HESSD

10, 1127–1183, 2013

with $k \approx 0.4$ being von Kármán's constant, and ψ_{sh} and ψ_{sm} correction terms for the actual stability conditions of the atmosphere (Brutsaert, 1982).

Despite the many non-measurable or unknown variables of Eq. (16), this is no dead end: the concept is not to parameterize a model by remotely sensed temperatures, but to utilize the data for additional spatial calibration. Thus, a global model adjustment to meet the water balance of the entire basin is a neccessary prerequisite.

Using Eqs. (14) and (15), one can express the basin average of actual evapotranspiration $\overline{ET_a}$ by integrating over the basin area A, regarding R_n, ΔT, and r_{ah} as functions of the co-ordinates x and y:

$$\overline{ET_a} = \frac{1}{\lambda \cdot A} \left(\iint\limits_A R_n(x,y)\,dA - \varrho_a c_p \iint\limits_A \frac{\Delta T(x,y)}{r_{ah}(x,y)}\,dA \right) \tag{17}$$

Assuming a well calibrated model, the modelled evapotranspiration height, denoted by ET_{SWIM}, equals the real spatial mean of ET_a, and integrating the spatially varying fluxes could practically be done by summing up the contributions of the n model hydrotopes with areas a_i:

$$\overline{ET_a} = ET_{SWIM} = \frac{1}{\lambda \cdot A} \left(\sum_{i=1}^{n} R_{n,i} a_i - \varrho_a c_p \sum_{i=1}^{n} \frac{\Delta T_i a_i}{r_{ah,i}} \right) \tag{18}$$

Unfortunately, the aerodynamic resistances $r_{ah,i}$, of which each hydrotope has its own value, are still unknown and change with atmospheric conditions.

The simplest solution would be assuming one common resistance for the entire basin. But from Eq. (16), we know the factors which govern r_{ah}: while integrating many observations may approximate an atmospheric mean state which is unlikely to fluctuate on distances below the meteorological meso-γ-scale (i.e. below 200 km), the time-invariant land use pattern will definitely reverberate in the sensible heat flux via its surface structure. Therefore, the general approach taken here is to assume two different effective resistance values: $r_{ah,f}$ for the forested part of the basin and $r_{ah,n}$ for the

HESSD
10, 1127–1183, 2013

Three perceptions of the evapotranspiration landscape

T. Conradt et al.

rest of the domain, because forests differ most distinctively in their effective roughness and displacement heights from the remaining landscape. Elevation effects, including the strongly correlated wind effects, are neglected, and wind speed is not considered by SWIM either. But eventual elevation dependencies can and will be analysed from the results.

A first variant is double usage of Eq. (18): for the m forested and the remaining $n-m$ non-forested hydrotopes, relying on the modelled averages of the respective land cover evapotranspiration $\mathrm{ET}_{\mathrm{S},f} + \mathrm{ET}_{\mathrm{S},n} = \mathrm{ET}_{\mathrm{SWIM}}$. The resistance values can then be directly calculated as follows:

$$r_{\mathrm{ah},f} = \frac{\varrho_\mathrm{a} c_\mathrm{p} \sum_{i=1}^{m} \Delta T_i a_i}{\sum_{i=1}^{m} R_{n,i} a_i - \lambda \mathrm{ET}_{\mathrm{S},f} \cdot A_f} \tag{19}$$

$$r_{\mathrm{ah},n} = \frac{\varrho_\mathrm{a} c_\mathrm{p} \sum_{i=m+1}^{n} \Delta T_i a_i}{\sum_{i=m+1}^{n} R_{n,i} a_i - \lambda \mathrm{ET}_{\mathrm{S},n} \cdot A_n} \tag{20}$$

A second variant does not presuppose a bias-free evapotranspiration modelling regarding land use, but a number $k > 2$ of gauged sub-basins with different forest shares within the model domain. In this case, the long-term water balance of each sub-basin can be calculated from the measurements, and $r_{\mathrm{ah},f}$ and $r_{\mathrm{ah},n}$ are to be estimated by minimising the error terms ε in the over-determined equation system

$$\begin{aligned}
\mathrm{ET}_{\mathrm{a},s1} &= \frac{1}{\lambda \cdot A_{s1}} \left[\sum_{i=j1}^{m1} R_{\mathrm{n},i} a_i - \varrho_\mathrm{a} c_\mathrm{p} \left(\sum_{i=j1}^{m1} \frac{\delta_f \cdot \Delta T_i a_i}{r_{\mathrm{ah},f}} + \sum_{i=j1}^{m1} \frac{\delta_n \cdot \Delta T_i a_i}{r_{\mathrm{ah},n}} \right) \right] + \varepsilon_1 \\
\mathrm{ET}_{\mathrm{a},s2} &= \frac{1}{\lambda \cdot A_{s2}} \left[\sum_{i=j2}^{m2} R_{\mathrm{n},i} a_i - \varrho_\mathrm{a} c_\mathrm{p} \left(\sum_{i=j2}^{m2} \frac{\delta_f \cdot \Delta T_i a_i}{r_{\mathrm{ah},f}} + \sum_{i=j2}^{m2} \frac{\delta_n \cdot \Delta T_i a_i}{r_{\mathrm{ah},n}} \right) \right] + \varepsilon_2 \\
\vdots \quad &= \quad \vdots \quad + \vdots \\
\mathrm{ET}_{\mathrm{a},sk} &= \frac{1}{\lambda \cdot A_{sk}} \left[\sum_{i=jk}^{mk} R_{\mathrm{n},i} a_i - \varrho_\mathrm{a} c_\mathrm{p} \left(\sum_{i=jk}^{mk} \frac{\delta_f \cdot \Delta T_i a_i}{r_{\mathrm{ah},f}} + \sum_{i=jk}^{mk} \frac{\delta_n \cdot \Delta T_i a_i}{r_{\mathrm{ah},n}} \right) \right] + \varepsilon_k
\end{aligned} \tag{21}$$

HESSD
10, 1127–1183, 2013

with

$$\delta_f = \begin{cases} 1 \text{ for forested hydrotopes} \\ 0 \text{ for other land use} \end{cases} \quad (22)$$

$$\delta_n = 1 - \delta_f \quad (23)$$

The indices si with $i \in \{1,2,\ldots,k\}$ refer to the k sub-basins, and the respective $\{ji, ji+1, ji+2,\ldots,mi\}$ indicate the hydrotope numbers within these sub-basins.

2.2.3 From snapshots to annual values

Hitherto, nothing has been said about the time frame on which Eqs. (18ff) should be applied. Principally, a single day or several years make no difference, provided that effective temperature gradients for the entire period can be provided. Effective means that the difference between satellite-derived surface temperature and ground-measured air temperature must always be extrapolated from the snapshot time(s) of the actual measurements to a period average.

Assuming a linear relationship between simultaneously measured temperature gradients on different hydrotopes and their respective evapotranspiration rates, it is possible to calculate their individual evapotranspiration heights for any longer period provided the total ET is known, and relations between the hydrotopes' aerodynamic resistances remain invariant. This works with averages of the ΔT observations for each hydrotope, denoted by overline; the index k refers to the selected hydrotope:

$$\mathrm{ET}_{\mathrm{a},k} = \mathrm{ET}_{\mathrm{tot}} \cdot \frac{A\left(R_{\mathrm{n},k} - \overline{\Delta T}_k \frac{\varrho_\mathrm{a} c_\mathrm{p}}{r_{\mathrm{ah},k}}\right)}{\sum_{i=1}^{n} a_i \left(R_{\mathrm{n},i} - \overline{\Delta T}_i \frac{\varrho_\mathrm{a} c_\mathrm{p}}{r_{\mathrm{ah},i}}\right)} \quad (24)$$

It makes hardly any difference whether the measurements were taken at noon or in late afternoon, as long as R_n was positive and dominant compared to G, but note that the resistances r_ah have to be fitted accordingly.

HESSD
10, 1127–1183, 2013

2.3 The water balance method

The classical water balance equation reads:

$$P = \mathrm{ET} + Q + \Delta S \qquad (25)$$

Evapotranspiration ET should theoretically equal precipitation P minus discharge Q for time scales of several years, because ΔS, the change in water storage of the catchment, gets neglectable compared to the other variables within such a time-span.

Practically, this approach has to grapple with difficulties in measuring catchment precipitation and uncertainties about catchment boundaries; the latter includes unaccounted ground water exchanges with neighbouring areas. The measured discharge may even be influenced by anthropogenic management. But due to lack of better alternatives, the water balance approach is commonly accepted as reference assessment of long-term mean evapotranspiration for river basins.

3 Results

The eco-hydrological model SWIM, only globally calibrated on the daily runoff values of the 1990s at the outlet gauge Neu Darchau, was run for the three years 2001–2003. Using the simulated ET averages from forested and non-forested hydrotopes, 944 remotely sensed land surface temperature (LST) maps from this period were evaluated. The area-averaged general results of this calculation are summarised in Table 1.

3.1 Application of the remote sensing method

The LST maps derived from NOAA AVHRR thermal imagery were readily provided by the German DLR Applied Remote Sensing Cluster and could be downloaded via its EOWEB portal (http://www.eoweb.de). These maps cover whole Europe at a resolution of approximately 1.1 km in the map centre. There are several AVHRR products made

HESSD
10, 1127–1183, 2013

available this way: two LST maps for each day from daylight and nighttime overpasses, a daily vegetation index (NDVI) map, and composite products for weeks and months. This study utilizes all 944 available daytime LST maps of the years 2001–2003.

Detailed information on these data is given by Tungalagsaikhan and Guenther (2007), including cloud screening procedures and the algorithms applied for computing the LST values from the thermal radiances. The latter had originally been established by Becker and Li (1990) and van de Griend and Owe (1993), and they were proven to be superior to other methods for this part of the world.

The European LST maps were reprojected onto the hydrotope map of the SWIM model, and mean surface temperatures could be calculated for each hydrotope when completely free from cloud cover. Hence, a first problem arises: how to deal with spatio-temporally varying cloud coverage?

Figure 3 demonstrates that the scanning times of the LST maps vary heavily due to satellite orbit characteristics and an intermediate change of the platform. Regarding the ground-measured air temperatures, only three measurements per day were available from the climate stations: minimum, maximum and average temperature. The maximum values, interpolated to sub-basin resolution, had to serve as best estimate for T_a at satellite overpass time.

Here, average temperature gradients had to be determined for the three calender years 2001–2003. One possible approach could be averaging only the seven days having LST maps with less than one per cent cloud cover. But 732 out of the 944 maps show surface temperatures for more than one per cent of the basin – and their information should not be discarded. The solution applied here is to produce a composite map of temperature gradients by averaging all available daily ΔT values for each hydrotope and correcting them for cloud cover frequencies as described below.

Figure 4 shows both the blue-sky fractions of the satellite maps and the simulated evapotranspiration for the model domain of SWIM. Luckily, there is a correspondence: especially in wintertime, when the remote sensing information suffers from permanent cloud and snow coverage, or the longer data gap occured, there is only small evapotranspiration. Therefore, no time-dependent weighting scheme to fit LST (and hence ΔT) observation frequencies to evapotranspiration intensities had been applied, and snow cover effects could be neglected.

On the other hand, the spatial pattern of cloudiness shown in Fig. 5 had to be considered. Radiation and accordingly heat gradients and evapotranspiration rates are much lower under cloud cover compared to blue sky conditions.

The cloud screening procedure applied by DLR prohibits LST calculations as soon as the respective pixel is cloud contaminated (Tungalagsaikhan and Guenther, 2007), i. e., is not totally cloud-free. White pixels include all conditions from thin cirrus with hardly dimmed radiation to dense stratus. A "blue-sky gradient" ΓT was calculated for each hydrotope observation without any white pixels (i.e. for the shares shown in Fig. 5a). The effective temperature gradient ΔT could then be estimated with the average blue-sky fraction of the hydrotope β, shown in Fig. 5b, assuming a mean attenuation factor of $\eta = 0.33$ of the cloud layer in white pixels:

$$\Delta T = \beta \cdot \Gamma T + \eta(1-\beta) \cdot \Gamma T \tag{26}$$

Although the value of η plays an important role for the range of these gradients, the resulting ET heights are hardly sensitive to it; the relative pattern remains quite stable for different choices of η, and the total evapotranspiration sum is kept to the level obtained from the hydrological model by an appropriate adjustment of the aerodynamic resistances r_{ah}.

The resulting map of average temperature gradients is shown in Fig. 6. Mountainous regions, wetlands, or regions with many lakes (near the catchment boundary in the north) are clearly distinguishable by values close to zero. The most extreme gradients were determined for lowland areas in the north of the Czech Republic. This is most probably an artifact due to the sparseness of climate station data in that region.

In 2001 the German part of the Elbe basin experienced an average year regarding radiation and precipitation, 2002 was warm and relatively wet (an extreme flood occurred in August), and in 2003 the vegetation period was exceptionally dry, sunny, and hot

HESSD
10, 1127–1183, 2013

(Müller-Westermeier et al., 2002; Müller-Westermeier and Rieke, 2003, 2004). This sequence can be confirmed by the ET simulations and average temperature gradients; cf. Table 1. The variations in the resistance values can be explained by respective subsequent increases in the numerators of Eqs. 19 and 20 combined with an increase in the denominators (more R_n, less ET) between 2002 and 2003. The resistance values are also sensitive to the adjustment of η: with $\eta = 0.25$ instead of 0.33, the time-averaged $r_{ah,f}$ decreases from 99.2 to 87.3 $s\,m^{-1}$ and $r_{ah,n}$ from 103.6 to 85.4 $s\,m^{-1}$. But in any case, the aerodynamic resistances range in the order of magnitude for vegetated surfaces in temperate climate found by many other authors (e.g. Thom and Oliver, 1977; Lindroth, 1993; Ramakrishna and Running, 1989; Liu et al., 2007).

3.2 Comparison of the three methods' results

Figures 7 to 9 present the patterns of the three ET estimations for the 133 gauged sub-basins in three respective maps, and Fig. 10 shows the sub-basin estimations in three scatter plots for the possible pair combinations of the three methods. The first main message is that the variances of both ground corrected and remotely sensed ET clearly exceed those of the simulation results from the only globally calibrated hydrological model.

The second insight delivered from Fig. 10 is that there is a weak correlation between the model and the remote sensing approach, an even weaker agreement between model and ground based validation, and, finally, practically no relationship between remote sensing and the water balance approach.

In order to shed light into the discrepancy between water balance and remote sensing estimations, we grouped those sub-basins which deviate most from being correlated in the lower right panel of Fig. 10 into clusters and highlighted them in a map. The clustering and its geospatial correspondence are shown in Fig. 11.

It turns out that all “deviating” sub-basins are located in the Czech part of the Elbe basin. The cluster of sub-basins marked by red colour which combine low remotely sensed ET with medium to high ET found by the water balance method concentrate in

Discussion Paper | Discussion Paper | Discussion Paper | Discussion Paper |

HESSD

10, 1127–1183, 2013

Three perceptions of the evapotranspiration landscape

T. Conradt et al.

the lowlands of the northwestern part of the Czech republic, while the opposite combination coloured in blue with high remotely sensed ET values was found at sub-basins distributed around the mountainous edge of the Czech area.

Subsetting the data to the 72 German sub-basins clearly increases all correlations as presented in Fig. 12. The upper left panel of Fig. 12 shows a relatively good agreement between ET estimates of the remotely sensed approach and the globally calibrated model simulation. Outliers are dominated by smaller sub-basins which could be expected (cf. the Introduction).

Our second, independent "ground truth" given by the water balance estimations of evapotranspiration for the sub-basins shows at least little correlation with SWIM and, at least in the German subset, also with the remotely sensed ET (compare the lower panels in Figs. 10 and 12).

While restricting the data basis to the German sub-basins decreased the variance of the remotely sensed ET heights, the water balance based estimations still cover a comparably wide range. Again, systematical errors can be identified by mapping the most prominent outliers in the lower right panel of Fig. 12, this is done in Fig. 13.

It appears that two pairs of subsequent gauge areas at the lower Havel River (Ketzin and Rathenow) and at the Elbe River downstream the Havel (Wittenberge and Neu Darchau) have both been assigned combinations of very low and high ET estimates from the water balance method.

4 Discussion

4.1 Remote sensing estimations

The explanation for the heavy noise in the remote sensing estimations for Czech sub-basins is the low density of ground measurements there: the geospatial pattern of the outlier sub-basins in Fig. 11 matches that of the most extreme temperature gradients in Fig. 6. Taking into account that the spatial density of climate stations of which data

HESSD
10, 1127–1183, 2013

were provided was much lower in the Czech part than in the rest of the basin (only 46 out of the 853 stations were located there), it is highly probable that the 2 m air temperature and hence the resulting temperature gradient were systematically biased preventing the remote sensing approach from working properly in this region.

The remaining noise of the remote sensing results in Fig. 12 is in the range observed by most recent studies evaluating remotely sensed ET by some kind of "ground truth", be it reference ET calculated from lysimeter measurements (Wloczyk, 2007; Sánchez et al., 2008), eddy flux or other micrometeorological tower measurements (Verstraeten et al., 2005; Patel et al., 2006; McCabe and Wood, 2006; Brunsell et al., 2008; de C. Teixeira et al., 2009), or hydrological model simulations (Boegh et al., 2004; Gao and Long, 2008; Galleguillos et al., 2011).

An exception is the study by Immerzeel and Droogers (2008), who calibrated a SWAT application by the remotely sensed evapotranspiration pattern: their scatter-plot of reference ET for 115 model sub-basins simulated without spatial calibration against respective SEBAL results does not show a visible correlation; the numerical value is not given.

4.2 Water balance estimations

The reason for the outliers in the water balance estimation for subsequent gauges (cf. Fig. 13) are slightly biased discharge measurements causing sweeping oscillating errors.

For example, the inflow from upstream into the area assigned to gauge Wittenberge has a long-term mean of about 695 $m^3 s^{-1}$. Downstream at gauge Neu Darchau the respective value amounts to 760 $m^3 s^{-1}$. At gauge Wittenberge, right between these rather equally sized contribution areas, one would expect a mean runoff of about 727.5 $m^3 s^{-1}$. But 737 $m^3 s^{-1}$ is taken as "correct" measurement there. This is just a deviation of 1.3 % and clearly within gauging uncertainty (cf. Sauer and Meyer, 1992; Maniak, 2005). But this relatively little shift would mean a discharge of 42 $m^3 s^{-1}$ from the area above Wittenberge and only 23 $m^3 s^{-1}$ from the area below. The climate for

HESSD
10, 1127–1183, 2013

both patches does not differ very much, the latter receives even a little more precipitation. Consequently, a rather low evapotranspiration rate is calculated for the area above Wittenberge and a much higher one for the Neu Darchau area. Finally, this leads to the picture shown in Fig. 13.

The case for Ketzin and Rathenow is very much the same. In general, measurement errors of subsequent gauges on the same river renders reasonable water balancing impossible when the total runoff is relatively large compared to the discharge from the intermediate area.

Finally, the impacts of another probable error source shall be assessed: the massive anthropogenic ground water extraction from open-cast lignite mining areas that peaked in the 1980s when more than 30 $m^3 s^{-1}$ excess flow were lead into the Spree River Grünewald (2001). In Fig. 14, the sub-basins whose discharges were presumably elevated by pumped ground water are coloured according to their river catchment affiliation.

One would expect too low ET estimations for open-cast mining affected sub-basins, which would (wrongly) explain their elevated discharge. Figure 14 shows that this holds only true for some sub-basins contributing to the Spree River, drawn in red. For the Pleiße sub-basin (yellow/orange) the plot reveals no visible effect, and the blue-coloured sub-basins of the Schwarze Elster River catchment seem to be drifted towards ET over-estimation.

The Schwarze Elster sub-basins demonstrate the imponderabilities in accounting for open cast mining effects on discharge. While the pumping rates have been thoroughly measured by water meters, natural ground water contributions to streamflow diminished or ceased to a largely unknown extent. Because the ground water pumping into the Schwarze Elster had seen its maximum rates already in the 1960s before most sub-basin gauges went into operation, reduced discharges due to the already generated groundwater deficit are likely to have dominated the calibration periods.

HESSD
10, 1127–1183, 2013

4.3 Eco-hydrological model simulations

The output of the SWIM simulations are of course also subject to errors. The model water balances of two groups of hydrotopes – forested and non-forested – were taken for adjusting the remote sensing based ET values which might have added to the overall noise of the results. It has to be pointed out that the internally computed LAI values were left unmodified, although some standard parameterisations for land cover units are questionable for parts of the model domain; e.g. the Ore Mountains. There had been a severe forest dieback in the crest region in the 1980s, but an ideal forest had been modelled.

The breakdown of the socialist economies in Eastern Europe around 1990 had global impacts on evapotranspiration via the phenomena of global dimming and brightening (Wild, 2012). This is relevant, because the eco-hydrological model was calibrated on data from before the change (Conradt et al., 2012b) when global radiation and ET were generally lower while the satellite scans were taken under brightening conditions. It remains unclear, to what extent different land uses were affected differently, but individually changing Bowen-ratios might also have contributed to the observed uncertainties.

Finally, it has to be noted that the modelling of lateral water exchanges between sub-basins was limited to stream runoff. Groundwater exchanges affecting plant water availability and thus ET were not considered.

5 Conclusions

The comparison of three independent estimations for the spatial evapotranspiration pattern within the Elbe River basin – the semi-distributed model SWIM, the remote sensing approach, and the water balance method – delivered the key finding of this study: the water balance approach does not seem to be more exact than the two other methods. The relatively strong correlation between the modelled and the remotely

HESSD

10, 1127–1183, 2013

Three perceptions of the evapotranspiration landscape

T. Conradt et al.

sensed estimates tells indeed the opposite, which is meaningful, because the ground based approach is commonly trusted most.

Concerning the recently published climate change impact study for the Elbe River basin (Wechsung et al., 2013) which relies on ground-based spatial calibration (Conradt et al., 2012a,b, 2013a,b), the consequence of our findings has to be extra caution when interpreting the results; cf. the assessments of water management options (Kaltofen et al., 2013a,b; Koch et al., 2013a,b) and the related economic consequences (Grossmann et al., 2013).

5.1 Sources of uncertainty

There are several reasons which have disturbed the validity of the water balance derived evapotranspiration heights, two of them have been shown explicitly. They can be divided up into aleatoric (driven by randomness) and epistemic (caused by lack of knowledge) uncertainties. The following list contains also other likely sources of uncertainty and is not meant to be exhaustive:

A. Aleatoric uncertainties

1. Biased interpolation of climate data in sparsely instrumented areas
2. Errors of gauge measurements along major streams affecting intermediate areas

B. Epistemic uncertainties

3. Unknown groundwater fluxes between adjoining sub-basins
4. Unknown artificial water transfers between sub-basins
5. Erroneous or missing provision for the impacts of mining

While we could detect both aleatoric uncertainties listed above, the epistemic examples are natural starting points for further research. Of course, experiences or findings of other studies give some clues for the items in second part of the list.

Discussion Paper | Discussion Paper | Discussion Paper | Discussion Paper |

HESSD

10, 1127–1183, 2013

Three perceptions of the evapotranspiration landscape

T. Conradt et al.

Title Page

Abstract Introduction

Conclusions References

Tables Figures

◀◀ ▶▶

◀ ▶

Back Close

Full Screen / Esc

Printer-friendly Version

Interactive Discussion

For example, the assumption of hidden, unaccounted groundwater fluxes is not at all implausible for the lowlands with their dominating sandy sediments. Although significant effects are more likely for small areas, Schaller and Fan (2009) postulated groundwater export or import altering the water balances even for large basins (up to $\approx 50\,000\,\mathrm{km}^2$) in the United States.

For lowland rivers in subcatchments of the Elbe River basin, Krause and Bronstert (2007) and Krause et al. (2007) investigated and modelled variable interactions between groundwater and surface water. Their findings question directly the credibility of both the SWIM model and the water balance approach for smaller sub-basins in this landscape. Additionally, many lowland areas of the Elbe River basin are covered with a network of ditches and canals, and their impact is sparsely known.

5.2 Perceptions of reality

Because differences between remotely sensed hydrological properties and any kind of validation data are so widespread and frequently observed, it is easy to speak of distinct perceptions of reality. Great efforts have been made to merge these differing views into one consistent picture of reality. At present, the most prominent research field is data assimilation (Evensen, 2007; Liu and Gupta, 2007; Mathieu and O'Neill, 2008; Reichle, 2008). Practical examples for integrating evapotranspiration patterns retrieved by remote sensing into hydrological modelling give Pan et al. (2008); Qin et al. (2008); Long and Singh (2010); Schuurmans et al. (2011), or Liu et al. (2012), but how about the difference between (merged) perception and reality?

The core concept of data fusion or data assimilation (e.g. by Kalman filtering) – providing best estimates of real values by weighted means of the diverging input data – may lead to biased results, because any weighting is subject to prior assumptions on the error variances of the input data; cf. van Leeuven and Evensen (1996) or McLaughlin (2002) for details about the Bayesian background. The concept may even not be applicable at all when systematic errors override the information content expected from a certain data source. McCabe et al. (2008) quite correspondingly conclude that while

HESSD
10, 1127–1183, 2013

achieving hydrological consistency is urgently needed for improving hydrological prediction, there is currently no comprehensive or robust framework for integrating a multitude of observations; simply developing more efficient merging techniques would not be the key issue. Some attempts have at least been made; an example is given by Vrugt et al. (2005) who combined global optimisation and sequential data assimilation in a hybrid framework.

5.3 Recommendations

Despite these challenges, incorporating additional information by means of remote sensing must be strongly recommended for any distributed modelling project: In any case, it can serve as independent spatial basis of comparison, and only by investigating the differences rather than by interpolating them away, modelling may come closer to reality.

However, our approach of combining remotely sensed with ground measured data for estimating evapotranspiration can only be recommended for areas with high density of meteorological stations. Otherwise, poor performance prevents any meaningful assessment, and an alternative method like SEBAL (Bastiaanssen et al., 1998a,b) should be used instead.

Meteorological and stream gauge measurements will of course remain the bread and butter for driving and calibrating hydrological models. But with the experience of heavily deviating water balances in sub-basins, more care should be taken with respect to probable lateral water fluxes.

If there are only few runoff data from interior stream gauges, a distributed hydrological model can be spatially calibrated on remotely sensed ET patterns, but to achieve realistic discharge simulations in space, additional local knowledge, e.g. on groundwater exchange and water management effects, is essential. If there are many data from a lot of interior gauges, a comparison with remotely sensed ET patterns should always be used to identify local pecularities and to customise the model, respectively.

HESSD
10, 1127–1183, 2013

Finally, this endorses the case made by Beven (2001): the future of hydologic science lies less in the development of new theories and models but in gathering knowledge and understanding about specific areas; it should rather be a “learning about places” (see also Beven, 2003, 2007).

Acknowledgements. We are grateful to Jakob P. Köhler and Stefan Lange for downloading most of the 944 LST map images and to Peter Seifert from DLR for technical assistance in this lengthy process. This work was compiled within the framework of the German GLOWA-Elbe research project (http://www.glowa-elbe.de) funded by the German Ministry for Education and Research (BMBF, http://www.bmbf.de), grant no. 01 LW 0603 A2.

References

Ajami, N. K., Gupta, H., Wagener, T., and Sorooshian, S.: Calibration of a semi-distributed hydrologic model for streamflow estimation along a river system, J. Hydrol., 298, 112–135, doi:10.1016/j.jhydrol.2004.03.033, 2004. 1128

Albertz, J.: Grundlagen der Interpretation von Luft- und Satellitenbildern, Wissenschaftliche Buchgesellschaft, Darmstadt, 1991. 1138

Andersen, J., Refsgaard, J. C., and Jensen, K. H.: Distributed hydrological modelling of the Senegal River Basin – model construction and validation, J. Hydrol., 247, 200–214, doi:10.1016/S0022-1694(01)00384-5, 2001. 1128

Andréassian, V., Lerat, J., Loumagne, C., Mathevet, T., Michel, C., Oudin, L., and Perrin, C.: What is really undermining hydrologic science today?, Hydrol. Process., 21, 2819–2822, doi:10.1002/hyp.6854, 2007. 1129

Andréassian, V., Le Moine, N., Perrin, C., Ramos, M.-H., Oudin, L., Mathevet, T., Lerat, J., and Berthet, L.: All that glitters is not gold: the case of calibrating hydrological models, Hydrol. Process., 26, 2206–2210, doi:10.1002/hyp.9264, 2012. 1129

Arnold, J. G., Allen, P. M., and Bernhardt, G.: A comprehensive surface-groundwater flow model, J. Hydrol., 142, 47–69, doi:10.1016/0022-1694(93)90004-S, 1993. 1134

Arnold, J. G., Srinivasan, R., Muttiah, R. S., and Williams, J. R.: Large area hydrologic modeling and assessment Part I: Model development, J. Am. Water Resour. As., 34, 73–89, doi:10.1111/j.1752-1688.1998.tb05961.x, 1998. 1134

HESSD

10, 1127–1183, 2013

Three perceptions of the evapotranspiration landscape

T. Conradt et al.

ATV-DVWK: Verdunstung in Bezug zu Landnutzung, Bewuchs und Boden, DWA-Merkblatt atv-dvwk-m 504, DWA Deutsche Vereinigung für Wasserwirtschaft, Abwasser und Abfall e. V., Hennef, 2002. 1136

Bastiaanssen, W. G. M., Menenti, M., Feddes, R. A., and Holtslag, A. A. M.: A remote sensing surface engergy balance algorithm for land (SEBAL). 1. Formulation, J. Hydrol., 212–213, 198–212, doi:10.1016/S0022-1694(98)00253-4, 1998a. 1131, 1137, 1154

Bastiaanssen, W. G. M., Pelgrum, H., Wang, J., Ma, Y., Moreno, J. F., Roerink, G. J., and van der Wal, T.: A remote sensing surface engergy balance algorithm for land (SEBAL). 2. Validation, J. Hydrol., 212–213, 213–229, doi:10.1016/S0022-1694(98)00254-6, 1998b. 1131, 1137, 1154

Becker, F. and Li, Z. L.: Towards a local split method over land surfaces, Int. J. Remote Sens., 11, 369–393, doi:10.1080/01431169008955028, 1990. 1145

Bergström, S. and Graham, L. P.: On the scale problem in hydrological modelling, J. Hydrol., 211, 253–265, doi:10.1016/S0022-1694(98)00248-0, 1998. 1129

Beven, K.: Changing ideas in hydrology – the case of physically-based models, J. Hydrol., 105, 157–172, doi:10.1016/0022-1694(89)90101-7, 1989. 1129

Beven, K.: The limits of splitting: hydrology, Sci. Total Environ., 183, 89–97, doi:10.1016/0048-9697(95)04964-9, 1996. 1129, 1131

Beven, K.: How far can we go in distributed hydrological modelling?, Hydrol. Earth Syst. Sci., 5, 1–12, doi:10.5194/hess-5-1-2001, 2001; EGS Dalton Lecture, 2001. 1131, 1155

Beven, K.: Towards integrated environmental models of everywhere: uncertainty, data and modelling as a learning process, Hydrol. Earth Syst. Sci., 11, 460–467, doi:10.5194/hess-11-460-2007, 2007. 1155

Beven, K. J.: On environmental models of everywhere on the GRID, Hydrol. Process., 17, 171–174, doi:10.1002/hyp.5090, 2003. 1155

Bilbao, J. and Miguel, A. H. D.: Estimation of daylight downward longwave atmospheric irradiance under clear-sky and all-sky conditions, J. Appl. Meteorol. Clim., 46, 878–889, doi:10.1175/JAM2503.1, 2007. 1139

Blöschl, G.: Scaling in hydrology, Hydrol. Process., 15, 709–711, doi:10.1002/hyp.432, 2001. 1129

Boegh, E., Thorsen, M., Butts, M. B., Hansen, S., Christiansen, J. S., Abrahamsen, P., Hasager, C. B., Jensen, N. O., van der Keur, P., Refsgaard, J. C., Schelde, K., Soegaard, H., and Thomsen, A.: Incorporating remote sensing data in physically based distributed

HESSD
10, 1127–1183, 2013

Three perceptions of the evapotranspiration landscape

T. Conradt et al.

agro-hydrological modelling, J. Hydrol., 287, 279–299, doi:10.1016/j.jhydrol.2003.10.018, 2004. 1131, 1149

Bowen, I. S.: The ratio of heat losses by conduction and evaporation from any water surface, Ph. D. thesis, California Institute of Technology, Pasadena, CA, 12 pp., 1926a. 1140

Bowen, I. S.: The ratio of heat losses by conduction and evaporation from any water surface, Phys. Rev., 27, 779–787, doi:10.1103/PhysRev.27.779, 1926b. 1140

Bronstert, A., Bardossy, A., Bismuth, C., Buiteveld, H., Disse, M., Engel, H., Fritsch, U., Hundecha, Y., Lammersen, R., Niehoff, D., and Ritter, N.: Multi-scale modelling of land-use change and river training aspects on floods in the Rhine basin, River Res. Appl., 23, 1102–1125, doi:10.1002/rra.1036, erratum: River Res. Appl. 24, 353, doi:10.1002/rra.1074, 2007. 1130

Brunsell, N. A., Ham, J. M., and Owensby, C. E.: Assessing the multi-resolution information content of remotely sensed variables and elevation for evapotranspiration in a tall-grass prairie environment, Remote Sens. Environ., 112, 2977–2987, doi:10.1016/j.rse.2008.02.002, 2008. 1149

Brunt, D.: Notes on radiation in the atmosphere. I, Q. J. Roy. Meteor. Soc., 58, 389–418, doi:10.1002/qj.49705824704, 1932. 1139

Brutsaert, W.: Evaporation into the Atmosphere – Theory, History, and Applications, Kluver Academic Publishers, Dordrecht, 1982. 1141

Choi, M., Jacobs, J. M., and Kustas, W. P.: Assessment of clear and cloudy sky parameterizations for daily downwelling longwave radiation over different land surfaces in Florida, USA, Geophys. Res. Lett., 35, L20402, doi:10.1029/2008GL035731, 2008. 1139

Conradt, T., Kundzewicz, Z. W., Hattermann, F., and Wechsung, F.: Measured effects of new lake surfaces on regional precipitation, Hydrolog. Sci. J., 52, 936–955, doi:10.1623/hysj.52.5.936, 2007. 1133

Conradt, T., Hattermann, F. F., Koch, H., and Wechsung, F.: Precipitation or evapotranspiration? Bayesian analysis of potential error sources in the simulation of sub-basin discharges in the Czech Elbe River basin, Reg. Environ. Change, 12, 649–661, doi:10.1007/s10113-012-0280-y, 2012a. 1130, 1152

Conradt, T., Koch, H., Hattermann, F. F., and Wechsung, F.: Spatially differentiated management-revised discharge scenarios for an integrated analysis of multi-realisation climate and land use scenarios for the Elbe River basin, Reg. Environ. Change, 12, 633–648, doi:10.1007/s10113-012-0279-4, 2012b. 1129, 1130, 1151, 1152

Conradt, T., Koch, H., Hattermann, F. F., and Wechsung, F.: Szenariosimulationen des Wasserabflusses, in: Die Elbe und ihr Einzugsgebiet im globalen Wandel, Chapt. 2.3, edited by: Wechsung, F., Hartje, V., Kaden, S., Venohr, M., Hansjürgens, B., and Gräfe, P., Weißensee Verlag, Berlin, in press, 2013a. 1129, 1152

Conradt, T., Koch, H., Hattermann, F. F., and Wechsung, F.: Validierung von Lokalkorrekturen der Verdunstung bei den Szenariosimulationen des Wasserabflusses, in: Die Elbe und ihr Einzugsgebiet im globalen Wandel, Chapt. 2.4, edited by: Wechsung, F., Hartje, V., Kaden, S., Venohr, M., Hansjürgens, B., and Gräfe, P., Weißensee Verlag, Berlin, in press, 2013b. 1152

Das, T., Bárdossy, A., Zehe, E., and He, Y.: Comparison of conceptual model performance using different representations of spatial variability, J. Hydrol., 356, 106–118, doi:10.1016/j.jhydrol.2007.11.017, 2008. 1129

de C. Teixeira, A. H., Bastiaanssen, W. G. M., Ahmad, M. D., and Bos, M. G.: Reviewing SEBAL input parameters for assessing evapotranspiration and water productivity for the Low-Middle São Francisco River basin, Brazil – Part A: Calibration and validation, Agr. Forest Meteorol., 149, 462–476, doi:10.1016/j.agrformet.2008.09.016, 2009. 1149

DeMarchi, C., Xing, F., Croley, T., He, C., and Wang, Y.: Application of a distributed large basin runoff model to Lake Erie: model calibration and analysis of parameter spatial variation, J. Hydrol. Eng., 16, 193–202, doi:10.1061/(ASCE)HE.1943-5584.0000304, 2011. 1130

Doorenbos, J. and Pruitt, W. O.: Guidelines for Predicting Crop Water Requirements, no. 24 in FAO Irrigation And Drainage Papers, Food and Agriculture Organisation of the United Nations, Rome, revised edn., 1977. 1139

DVWK: Ermittlung der Verdunstung von Land- und Wasserflächen, dwa-Merkblatt DVWK-M 238, DWA Deutsche Vereinigung für Wasserwirtschaft, Abwasser und Abfall e. V., Hennef, 1996. 1135, 1139

Evensen, G.: Data Assimilation – The Ensemble Kalman Filter, Springer, Heidelberg, 2007. 1153

Feyen, L., Kalas, M., and Vrugt, J. A.: Semi-distributed parameter optimization and uncertainty assessment for large-scale streamflow simulation using global optimization, Hydrolog. Sci. J., 53, 293–308, doi:10.1623/hysj.53.2.293, 2008. 1129

FGG Elbe: Zusammenfassender Bericht der Flussgebietsgemeinschaft Elbe über die Analysen nach Artikel 5 der Richtlinie 2000/60/EG (A-Bericht), Tech. rep., Flussgebietsgemeinschaft Elbe, Magdeburg, 2005. 1132, 1133

HESSD
10, 1127–1183, 2013

Three perceptions of the evapotranspiration landscape

T. Conradt et al.

Finger, D., Pellicciotti, F., Konz, M., Rimkus, S., and Burlando, P.: The value of glacier mass balance, satellite snow cover images, and hourly discharge for improving the performance of a physically based distributed hydrological model, Water Resour. Res., 47, W07519, doi:10.1029/2010WR009824, 2011. 1130

Galleguillos, M., Jacob, F., Prévot, L., French, A., and Lagacherie, P.: Comparison of two temperature differencing methods to estimate daily evapotranspiration over a Mediterranean vineyard watershed from ASTER data, Remote Sens. Environ., 115, 1326–1340, doi:10.1016/j.rse.2011.01.013, 2011. 1137, 1149

Gao, Y. and Long, D.: Intercomparison of remote sensing-based models for estimation of evapotranspiration and accuracy assessment based on SWAT, Hydrol. Process., 22, 4850–4869, doi:10.1002/hyp.7104, 2008. 1149

Garatuza-Payan, J., Pinker, R. T., Shuttleworth, W. J., and Watts, C. J.: Solar radiation and evapotranspiration in northern Mexico estimated from remotely sensed measurements of cloudiness, Hydrolog. Sci. J., 46, 465–478, doi:10.1080/02626660109492839, 2001. 1137

Gassman, P. W., Reyes, M. R., Green, C. H., and Arnold, J. G.: The soil and water assessment tool: historical development, applications, and future research directions, T. ASABE, 50, 1211–1250, 2007. 1134

Githui, F., Selle, B., and Thayalakumaran, T.: Recharge estimation using remotely sensed evapotranspiration in an irrigated catchment in southeast Australia, Hydrol. Process., 26, 1379–1389, doi:10.1002/hyp.8274, 2012. 1132, 1134

Glenn, E. P., Doody, T. M., Guerschman, J. P., Huete, A. R., King, E. A., McVicar, T. R., Van Dijk, A. I. J. M., Van Niel, T. G., Yebra, M., and Zhang, Y.: Actual evapotranspiration estimation by ground and remote sensing methods: the Australian experience, Hydrol. Process., 25, 4103–4116, doi:10.1002/hyp.8391, 2011. 1131

Grayson, R. B., Moore, I. D., and McMahon, T. A.: Physically based hydrologic modeling: 2. Is the concept realistic?, Water Resour. Res., 28, 2659–2666, doi:10.1029/92WR01259, 1992. 1129

Grossmann, M., Koch, H., Lienhoop, N., Vögele, S., Mutafoğlu, K., Möhring, J., Dietrich, O., and Kaltofen, M.: Economic risks associated with low flows in the Elbe River Basin (Germany): an integrated economic-hydrologic approach to assess vulnerability to climate change, Reg. Environ. Change, submitted, 2013. 1152

Grünewald, U.: Water resources management in river catchments influenced by lignite mining, Ecol. Eng., 17, 143–152, doi:10.1016/S0925-8574(00)00154-3, 2001. 1133, 1150

Gómez, M., Olioso, A., Sobrino, J. A., and Jacob, F.: Retrieval of evapotranspiration over the Alpilles/ReSeDA experimental site using airborne POLDER sensor and a thermal camera, Remote Sens. Environ., 96, 399–408, doi:10.1016/j.rse.2005.03.006, 2005. 1137

Güntner, A.: Large-scale hydrological modelling in the semi-arid north-east of Brazil, Ph. D. thesis, Universität Potsdam, available at: http://www.pik-potsdam.de/research/publications/pikreports/.files/pr77.pdf, also published as PIK Report 77 at Potsdam Institute for Climate Impact Research; last accessed: October 2012, 2002. 1128

Hoedjes, J. C. B., Chehbouni, A., Jacob, F., Ezzahar, J., and Boulet, G.: Delivering daily evapotranspiration from remotely sensed instantaneous evaporative fraction over olive orchard in semi-arid Morocco, J. Hydrol., 354, 53–64, doi:10.1016/j.jhydrol.2008.02.016, 2008. 1137

Immerzeel, W. W. and Droogers, P.: Calibration of a distributed hydrological model based on satellite evapotranspiration, J. Hydrol., 349, 411–424, doi:10.1016/j.jhydrol.2007.11.017, 2008. 1131, 1134, 1149

Ivanov, N. N.: Estimation of the amount of evaporation, P. All-Union Geogr. Soc., 86, 189–195, 1954 (in Russian) 1135

Ivanov, V. Y., Vivoni, E. R., Bras, R. L., and Entekhabi, D.: Preserving high-resolution surface and rainfall data in operational-scale basin hydrology: a fully distributed physically-based approach, J. Hydrol., 298, 80–111, doi:10.1016/j.jhydrol.2004.03.041, 2004. 1128

Jacobs, J. M., Anderson, M. C., Friess, L. C., and Diak, G. R.: Solar radiation, longwave radiation and emergent wetland evapotranspiration estimates from satellite data in Florida, USA / Estimations à partir de données satellitales du rayonnement solaire, du rayonnement de grande longueur d'onde et de l'évapotranspiration d'une zone humide de Floride (EUA), Hydrolog. Sci. J., 49, 461–476, doi:10.1623/hysj.49.3.461.54352, 2004. 1137

Jhorar, R. K., Smit, A. A. M. F. R., Bastiaanssen, W. G. M., and Roest, C. W. J.: Calibration of a distributed irrigation water management model using remotely sensed evapotranspiration rates and groundwater heads, Irrig. Drain., 60, 57–69, doi:10.1002/ird.541, 2011. 1131

Jiang, L. and Islam, S.: Estimation of surface evaporation map over Southern Great Plains using remote sensing data, Water Resour. Res., 37, 329–340, doi:10.1029/2000WR900255, 2001. 1137

Kaltofen, M., Hentschel, M., Kaden, S., Dietrich, O., and Koch, H.: Wasserverfügbarkeit im deutschen Elbegebiet, in: Die Elbe und ihr Einzugsgebiet im globalen Wandel, Chapt. 3.1, edited by: Wechsung, F., Hartje, V., Kaden, S., Venohr, M., Hansjürgens, B., and Gräfe, P., Weißensee Verlag, Berlin, in press, 2013a. 1152

HESSD
10, 1127–1183, 2013

Kaltofen, M., Hentschel, M., Kaden, S., Dietrich, O., and Koch, H.: Modelling of water availability in the Elbe River basin and impacts of global change in the German part, Reg. Environ. Change, in preparation, 2013b. 1152

Khakbaz, B., Imam, B., Hsu, K., and Sorooshian, S.: From lumped to distributed via semi-distributed: Calibration strategies for semi-distributed hydrologic models, J. Hydrol., 418–419, 61–77, doi:10.1016/j.jhydrol.2009.02.021, 2012. 1130

Kite, G. W. and Droogers, P.: Comparing evapotranspiration estimates from satellites, hydrological models and field data, J. Hydrol., 229, 3–18, doi:10.1016/S0022-1694(99)00195-X, 2000. 1137

Kite, G. W. and Pietroniro, A.: Remote sensing applications in hydrological modelling, Hydrolog. Sci. J., 41, 563–591, doi:10.1080/02626669609491526, 1996. 1131

Klemeš, V.: Empirical and causal models in hydrology, in: Scientific Basis of Water Resource Management, edited by: Geophysics Study Committee, Geophysics Research Board, A. o. M. and Phys. Science, N. R. C., Studies in geophysics, National Academy Press, Washington, D. C., 95–104, 1982. 1129

Klemeš, V.: Conceptualization and scale in hydrology, J. Hydrol., 65, 1–23, doi:10.1016/0022-1694(83)90208-1, 1983. 1131

Klemeš, V.: Dilettantism in hydrology: transition or destiny?, Water Resour. Res., 22, 177S–188S, doi:10.1029/WR022i09Sp0177S, 1986. 1129

Klemeš, V.: A hydrological perspective, J. Hydrol., 100, 3–28, doi:10.1016/0022-1694(88)90179-5, 1988. 1131

Koch, H., Kaltofen, M., Kaden, S., and Grünewald, U.: Wasserverfügbarkeit im tschechischen Elbegebiet, in: Die Elbe und ihr Einzugsgebiet im globalen Wandel, Chapt. 3.2, edited by: Wechsung, F., Hartje, V., Kaden, S., Venohr, M., Hansjürgens, B., and Gräfe, P., Weißensee Verlag, Berlin, in press, 2013a. 1152

Koch, H., Kaltofen, M., Kaden, S., and Grünewald, U.: Effects of global change on water availability in the Czech Elbe region, Reg. Environ. Change, in preparation, 2013b. 1152

Koloskov, G., Mukhamejanov, K., and Tanton, T. W.: Monin–Obukhov length as a cornerstone of the SEBAL calculations of evapotranspiration, J. Hydrol., 335, 170–179, doi:10.1016/j.jhydrol.2006.11.010, 2007. 1137

Krause, S. and Bronstert, A.: The impact of groundwater–surface water interactions on the water balance of a mesoscale lowland river catchment in northeastern Germany, Hydrol. Process., 21, 169–184, doi:10.1002/hyp.6182, 2007. 1134, 1153

Krause, S., Bronstert, A., and Zehe, E.: Groundwater–surface water interactions in a North German lowland floodplain – implications for the river discharge dynamics and riparian water balance, J. Hydrol., 347, 404–417, doi:10.1016/j.jhydrol.2007.09.028, 2007. 1153

Krysanova, V., Müller-Wohlfeil, D.-I., and Becker, A.: Development and test of a spatially distributed hydrological/water quality model for mesoscale watersheds, Ecol. Model., 106, 261–289, doi:10.1016/S0304-3800(97)00204-4, 1998. 1134

Krysanova, V., Bronstert, A., and Müller-Wohlfeil, D.-I.: Modelling river discharge for large drainage basins: from lumped to distributed approach, Hydrolog. Sci. J., 44, 313–331, doi:10.1080/02626669909492224, 1999. 1134

Krysanova, V., Wechsung, F., Arnold, J., Srinivasan, R., and Williams, J.: SWIM (Soil and Water Integrated Model) User Manual, PIK Report 69, Potsdam Institute for Climate Impact Research, Potsdam, Germany, http://www.pik-potsdam.de/research/publications/pikreports/.files/pr69.pdf, last access: October 2012, 2000. 1134

Lewis, J. M.: The story behind the Bowen ratio, B. Am. Meteorol. Soc., 76, 2433–2443, doi:10.1175/1520-0477(1995)076<2433:TSBTBR>2.0.CO;2, 1995. 1140

Lindroth, A.: Aerodynamic and canopy resistance of short-rotation forest in relation to leaf area index and climate, Bound.-Lay. Meteorol., 66, 265–279, doi:10.1007/BF00705478, 1993. 1147

Liu, Shaomin, Lu, L., Mao, D., and Jia, L.: Evaluating parameterizations of aerodynamic resistance to heat transfer using field measurements, Hydrol. Earth Syst. Sci., 11, 769–783, doi:10.5194/hess-11-769-2007, 2007. 1147

Liu, T., Willems, P., Feng, X. W., Li, Q., Huang, Y., Bao, A. M., Chen, X., Veroustraete, F., and Dong, Q. H.: On the usefulness of remote sensing input data for spatially distributed hydrological modelling: case of the Tarim River basin in China, Hydrol. Process., 26, 335–344, doi:10.1002/hyp.8129, 2012. 1130, 1153

Liu, Y. and Gupta, H. V.: Uncertainty in hydrologic modeling: toward an integrated data assimilation framework, Water Resour. Res., 43, W07401, doi:10.1029/2006WR005756, 2007. 1153

Long, D. and Singh, V. P.: Integration of the GG model with SEBAL to produce time series of evapotranspiration of high spatial resolution at watershed scales, J. Geophys. Res., 115, D21128, doi:10.1029/2010JD014092, 2010. 1137, 1153

Maniak, U.: Hydrologie und Wasserwirtschaft – Eine Einführung für Ingenieure, Springer, Heidelberg, 5th Edn., 2005. 1149

HESSD
10, 1127–1183, 2013

Mathieu, P.-P. and O'Neill, A.: Data assimilation: from photon counts to Earth System forecasts, Remote Sens. Environ., 112, 1258–1267, doi:10.1016/j.rse.2007.02.040, 2008. 1153
McCabe, M. F. and Wood, E. F.: Scale influences on the remote estimation of evapotranspiration using multiple satellite sensors, Remote Sens. Environ., 105, 271–285, doi:10.1016/j.rse.2006.07.006, 2006. 1149
McCabe, M. F., Wood, E. F., Wójcik, R., Pan, M., Sheffield, J., Gao, H., and Su, H.: Hydrological consistency using multi-sensor remote sensing data for water and energy cycle studies, Remote Sens. Environ., 112, 430–444, doi:10.1016/j.rse.2007.03.027, 2008. 1153
McLaughlin, D.: An integrated approach to hydrologic data assimilation: interpolation, smoothing, and filtering, Adv. Water Resour., 25, 1275–1286, doi:10.1016/S0309-1708(02)00055-6, 2002. 1153
Merz, R., Parajka, J., and Blöschl, G.: Scale effects in conceptual hydrological modeling, Water Resour. Res., 45, W09405, doi:10.1029/2009WR007872, 2009. 1129
Mo, X., Pappenberger, F., Beven, K., Liu, S., de Roo, A., and Lin, Z.: Parameter conditioning and prediction uncertainties of the LISFLOOD-WB distributed hydrological model/Conditionnement de paramétrage et incertitudes de prévision du modèle hydrologique distribué LISFLOOD-WB, Hydrolog. Sci. J., 51, 45–65, doi:10.1623/hysj.51.1.45, 2006. 1129
Monin, A. S. and Obukhov, A. M.: Basic laws of turbulent mixing in the ground layer of the atmosphere, T. Geophys. Inst. Acad. Sci. USSR, 24, 163–187, 1954 (in Russian). 1140
Moran, M. S., Kustas, W. P., Vidal, A., Stannard, D. I., Blanford, J. H., and Nichols, W. D.: Use of ground-based remotely sensed data for surface energy balance evaluation of a semiarid rangeland, Water Resour. Res., 30, 1339–1349, doi:10.1029/93WR03064, 1994. 1137
Moussa, R., Chahinian, N., and Bocquillon, C.: Distributed hydrological modelling of a Mediterranean mountainous catchment – model construction and multi-site validation, J. Hydrol., 337, 35–51, doi:10.1016/j.jhydrol.2007.01.028, erratum: J. Hydrol., 345, 254, doi:10.1016/j.jhydrol.2007.08.012, 2007. 1129
Müller-Westermeier, G. and Rieke, W.: Die Witterung in Deutschland, in: Klimastatusbericht 2002, Deutscher Wetterdienst, Offenbach, 79–87, 2003. 1147
Müller-Westermeier, G. and Rieke, W.: Die Witterung in Deutschland, in: Klimastatusbericht 2003, Deutscher Wetterdienst, Offenbach, 71–78, 2004. 1147
Müller-Westermeier, G., Czeplak, G., and Kreis, A.: Die Witterung in Deutschland, in: Klimastatusbericht 2001, Deutscher Wetterdienst, Offenbach, 125–130, 2002. 1147

Nagler, P.: The role of remote sensing observations and models in hydrology: the science of evapotranspiration, Hydrol. Process., 25, 3977–3978, doi:10.1002/hyp.8436, preface to Special Issue, 2011. 1131

Pan, M., Wood, E. F., Wójcik, R., and McCabe, M. F.: Estimation of regional terrestrial water cycle using multi-sensor remote sensing observations and data assimilation, Remote Sens. Environ., 112, 1282–1294, doi:10.1016/j.rse.2007.02.039, 2008. 1153

Patel, N. R., Rakhesh, D., and Mohammed, A. J.: Mapping of regional evapotranspiration in wheat using Terra/MODIS satellite data/Cartographie de l'évapotranspiration régionale du blé grâce á des données satellitales Terra/MODIS, Hydrolog. Sci. J., 51, 325–335, doi:10.1623/hysj.51.2.325, 2006. 1137, 1149

Pechlivanidis, I. G., McIntyre, N. R., and Wheater, H. S.: Calibration of the semi-distributed PDM rainfall–runoff model in the Upper Lee catchment, UK, J. Hydrol., 386, 198–209, doi:10.1016/j.jhydrol.2010.03.022, 2010. 1129

Pokhrel, P. and Gupta, H. V.: On the use of spatial regularization strategies to improve calibration of distributed watershed models, Water Resour. Res., 46, W01505, doi:10.1029/2009WR008066, 2010. 1129

Pokhrel, P. and Gupta, H. V.: On the ability to infer spatial catchment variability using streamflow hydrographs, Water Resour. Res., 47, W08534, doi:10.1029/2010WR009873, 2011. 1130

Qin, C., Jia, Y., Su, Z. B., Zhou, Z., Qiu, Y., and Suhui, S.: Integrating remote sensing information into a distributed hydrological model for improving water budget predictions in large-scale basins through data assimilation, Remote Sens. Environ., 8, 4441–4465, doi:10.3390/s8074441, 2008. 1153

Ramakrishna, R. N. and Running, S. W.: Estimation of regional surface resistance to evapotranspiration from NDVI and Thermal-IR AVHRR data, J. Appl. Meteorol., 28, 276–284, doi:10.1175/1520-0450(1989)028<0276:EORSRT>2.0.CO;2, 1989. 1147

Reed, S., Koren, V., Smith, M., Zhang, Z., Moreda, F., Seo, D.-J., and DMIP Participants: Overall distributed model intercomparison project results, J. Hydrol., 298, 27–60, doi:10.1016/j.jhydrol.2004.03.031, 2004. 1129

Reichle, R. H.: Data assimilation methods in the Earth sciences, Adv. Water Resour., 31, 1411–1418, doi:10.1016/j.advwatres.2008.01.001, 2008. 1153

Richter, D.: Verdunstung, in: Klimadaten der Deutschen Demokratischen Republik – Ein Handbuch für die Praxis, Vol. 6 of Reihe B, Meteorologischer Dienst der Deutschen Demokratischen Republik, Potsdam, 1984. 1135

HESSD

10, 1127–1183, 2013

Three perceptions of the evapotranspiration landscape

T. Conradt et al.

Ritchie, J. T.: A model for predicting evaporation from a row crop with incomplete cover, Water Resour. Res., 8, 1204–1213, doi:10.1029/WR008i005p01204, 1972. 1136

Santhi, C., Kannan, N., Arnold, J. G., and Di Luzio, M.: Spatial calibration and temporal validation of flow for regional scale hydrologic modeling, J. Am. Water Resour. As., 44, 829–846, doi:10.1111/j.1752-1688.2008.00207.x, 2008. 1130

Sauer, V. B. and Meyer, R. W.: Determination of error in individual discharge measurements, Open-File Report 92-144, US Geological Survey, Norcross, Georgia, available at: http://pubs.usgs.gov/of/1992/ofr92-144/ (last access date: 22 January 2013), 1992. 1149

Schaller, M. F. and Fan, Y.: River basins as groundwater exporters and importers: Implications for water cycle and climate modeling, J. Geophys. Res.-Atmos., 114, D04103, doi:10.1029/2008JD010636, 2009. 1153

Schultz, G. A.: Parameter determination and input estimation in rainfall-runoff modelling based on remote sensing techniques, in: Water for the Future: Hydrology in Perspective, Proceedings of the International Symposium on Water for the Future held in Rome, April 1987, edited by: Rodda, J. C. and Matalas, N. C., no. 164 in IAHS Publications ("Red Books" series), IAHS Press, Wallingford, UK, 425–438, 1987. 1131

Schultz, G. A.: Remote sensing in hydrology, J. Hydrol., 100, 239–265, doi:10.1016/0022-1694(88)90187-4, 1988. 1131

Schuurmans, J. M., van Geer, F. C., and Bierkens, M. F. P.: Remotely sensed latent heat fluxes for model error diagnosis: a case study, Hydrol. Earth Syst. Sci., 15, 759–769, doi:10.5194/hess-15-759-2011, 2011. 1130, 1131, 1137, 1153

Seibert, J., Uhlenbrook, S., Leibundgut, C., and Halldin, S.: Multiscale calibration and validation of a conceptual rainfall-runoff model, Phys. Chem. Earth Pt. B, 25, 59–64, doi:10.1016/S1464-1909(99)00121-5, 2000. 1130

Singh, U. K., Ren, L., and Kang, S.: Simulation of soil water in space and time using an agro-hydrological model and remote sensing techniques, Agr. Water Manage., 97, 1210–1220, doi:10.1016/j.agwat.2010.03.002, 2010. 1131

Sivakumar, B.: Undermining the science or undermining Nature?, Hydrol. Process., 22, 893–897, doi:10.1002/hyp.7004, 2008. 1129

Smith, M. B., Koren, V., Reed, S., Zhang, Z., Zhang, Y., Moreda, F., Cui, Z., Mizukami, N., Anderson, E. A., and Cosgrove, B. A.: The distributed model intercomparison project – Phase 2: Motivation and design of the Oklahoma experiments, J. Hydrol., 418–419, 3–16, doi:10.1016/j.jhydrol.2011.08.055, 2012a. 1129

HESSD

10, 1127–1183, 2013

Three perceptions of the evapotranspiration landscape

T. Conradt et al.

Smith, M. B., Koren, V., Zhang, Z., Zhang, Y., Reed, S. M., Cui, Z., Moreda, F., Cosgrove, B. A., Mizukami, N., Anderson, E. A., and DMIP 2 Participants: Results of the DMIP 2 Oklahoma experiments, J. Hydrol., 418–419, 17–48, doi:10.1016/j.jhydrol.2011.08.056, 2012b. 1129

Srinivasan, R., Ramanarayanan, T. S., Arnold, J. G., and Bednarz, S. T.: Large area hydrologic modeling and assessment Part II: Model application, J. Am. Water Resour. As., 34, 91–101, doi:10.1111/j.1752-1688.1998.tb05962.x, 1998. 1134

Stisen, S., Sandholt, I., Norgaard, A., Fensholt, R., and Jensen, K. H.: Combining the triangle method with thermal inertia to estimate regional evapotranspiration – applied to MSG-SEVIRI data in the Senegal River basin, Remote Sens. Environ., 112, 1242–1255, doi:10.1016/j.rse.2007.08.013, 2008. 1137

Stisen, S., McCabe, M. F., Refsgaard, J. C., Lerer, S., and Butts, M. B.: Model parameter analysis using remotely sensed pattern information in a multi-constraint framework, J. Hydrol., 409, 337–349, doi:10.1016/j.jhydrol.2011.08.030, 2011. 1130

Sánchez, J. M., Scavone, G., Caselles, V., Valor, E., Copertino, V. A., and Telesca, V.: Monitoring daily evapotranspiration at a regional scale from Landsat-TM and ETM+ data: application to the Basilicata region, J. Hydrol., 351, 58–70, doi:10.1016/j.jhydrol.2007.11.041, 2008. 1149

Thom, A. S. and Oliver, H. R.: On Penman's equation for estimating regional evaporation, Q. J. Roy. Meteor. Soc., 103, 345–357, doi:10.1002/qj.49710343610, 1977. 1147

Tungalagsaikhan, P. and Guenther, K. P.: NOAA AVHRR Derived Land Surface Temperature Maps (LST) – Source, Image Characteristics, and Processing, online publication, available at: http://eoweb.dlr.de/short_guide/D-LST.html, last access: September 2012, 2007. 1145, 1146

Turc, L.: Évaluation des besoins en eau d'irrigation, évaporation potentielle, Ann. Agron., 12, 13–49, 1961 (in French). 1135

van de Griend, A. A. and Owe, M.: On the relationship between thermal emissivity and the normalised difference vegetation index for natural surfaces, Int. J. Remote Sens., 14, 1119–1131, doi:10.1080/01431169308904400, 1993. 1145

van Dijk, A. I. J. M. and Renzullo, L. J.: Water resource monitoring systems and the role of satellite observations, Hydrol. Earth Syst. Sci., 15, 39–55, doi:10.5194/hess-15-39-2011, 2011. 1131 van Leeuven, P. J. and Evensen, G.: Data assimilation and inverse methods in terms of a probabilistic formulation, Mon. Weather Rev., 124, 2898–2913, doi:10.1175/1520-0493(1996)124<2898:DAAIMI>2.0.CO;2, 1996. 1153

Verstraeten, W. W., Veroustraete, F., and Feyen, J.: Estimating evapotranspiration of European forests from NOAA-imagery at satellite overpass time: towards an operational processing chain for integrated optical and thermal sendor data products, Remote Sens. Environ., 96, 256–276, doi:10.1016/j.rse.2005.03.004, 2005. 1137, 1149

Vinukollu, R. K., Sheffield, J., Wood, E. F., Bosilovich, M. G., and Mocko, D.: Multimodel analysis of energy and water fluxes: intercomparison between operational analyses, a land surface model, and remote sensing, J. Hydrometeorol., 13, 3–26, doi:10.1175/2011JHM1372.1, 2012. 1131

Vrugt, J. A., Diks, C. G. H., Gupta, H. V., Bouten, W., and Verstraten, J. M.: Improved treatment of uncertainty in hydrologic modeling: combining the strengths of global optimization and data assimilation, Water Resour. Res., 41, W01017, doi:10.1029/2004WR003059, 2005. 1154

Wechsung, F., Hartje, V., Kaden, S., Venohr, M., Hansjürgens, B., and Gräfe, P. (Eds.): Die Elbe und ihr Einzugsgebiet im globalen Wandel, Weißensee Verlag, Berlin, in press, 2013. 1152

Wendling, U. and Schellin, H.-G.: Neue Ergebnisse zur Berechnung der potentiellen Evapotranspiration, Z. Meteorol., 36, 214–217, 1986. 1135

Wild, M.: Enlightening global dimming and brightening, B. Am. Meteorol. Soc., 93, 27–37, doi:10.1175/BAMS-D-11-00074.1, 2012. 1151

Williams, J. R. and Hann, R. W.: Optimal operation of large agricultural watersheds with water quality constraints, Tech. Rep. 96, Texas Water Resources Institute, Texas A&M University, College Station, TX, 1978. 1136

Wloczyk, C.: Entwicklung und Validierung einer Methodik zur Ermittlung der realen Evapotranspiration anhand von Fernerkundungsdaten in Mecklenburg-Vorpommern, Ph. D. thesis, Universität Rostock, Agrar- und Umweltwissenschaftliche Fakultät, 2007. 1137, 1149

Wright, J. L. and Jensen, M. E.: Peak water requirements of crops in Southern Idaho, J. Irr. Drain. Div.-ASCE, 98, 193–201, 1972. 1139

Xie, H., Longuevergne, L., Ringler, C., and Scanlon, B. R.: Calibration and evaluation of a semi-distributed watershed model of Sub-Saharan Africa using GRACE data, Hydrol. Earth Syst. Sci., 16, 3083–3099, doi:10.5194/hess-16-3083-2012, 2012. 1130

HESSD
10, 1127–1183, 2013
Three perceptions of the evapotranspiration landscape
T. Conradt et al.

Title Page
Abstract | Introduction
Conclusions | References
Tables | Figures
◂ | ▸
Back | Close
Full Screen / Esc
Printer-friendly Version
Interactive Discussion

Zhang, X., Srinivasan, R., and Van Liew, M.: Multi-site calibration of the SWAT model for hydrologic modeling, T. ASABE, 51, 2039–2049, 2008. 1130

Zhang, X., Srinivasan, R., and Van Liew, M.: On the use of multi-algorithm, genetically adaptive multi-objective method for multi-site calibration of the SWAT model, Hydrol. Process., 24, 955–969, doi:10.1002/hyp.7528, 2010. 1130

HESSD

10, 1127–1183, 2013

Table 1. General results of the evapotranspiration calculation. The total area (134 890 km^2) is the modelled part of the Elbe River basin as shown in Figs. 7–9.

		Forested				Non-Forested			
A	km^2	42 590				92 300			
		2001	2002	2003	All*	2001	2002	2003	All*
ET	$mm\,a^{-1}$	664	693	557	638	503	541	490	511
R_n	$MJ\,m^{-2}\,a^{-1}$	1984	2001	2307	2098	2012	2014	2319	2115
ΔT	K	0.63	1.30	1.86	1.32	1.08	2.13	3.13	2.22
r_{ah}	$s\,m^{-1}$	71.0	171.5	79.2	99.2	55.5	124.5	112.5	103.6

* "All" refers to the results for the full data set of the three years 2001–2003.

HESSD
10, 1127–1183, 2013

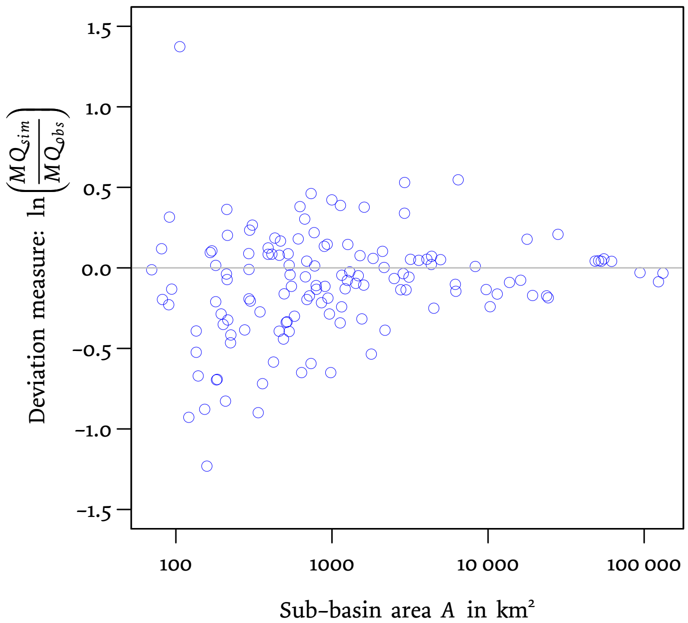

Fig. 1. Dependency of model discharge deviation on sub-basin size. For compatibility of positive and negative deviations, the logarithm of the relation of simulated to measured mean discharge has been used as error measure.

HESSD

10, 1127–1183, 2013

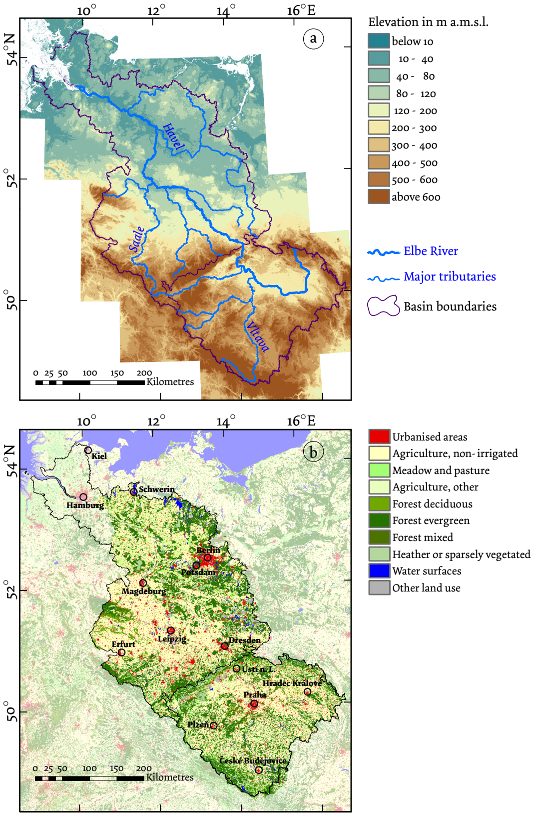

Fig. 2. The Elbe basin in central Europe: **(a)** Elevations and major tributary streams. **(b)** Land use according to the CORINE 2000 classification; saturated tints indicate the model domain.

HESSD
10, 1127–1183, 2013

Three perceptions of the evapotranspiration landscape

T. Conradt et al.

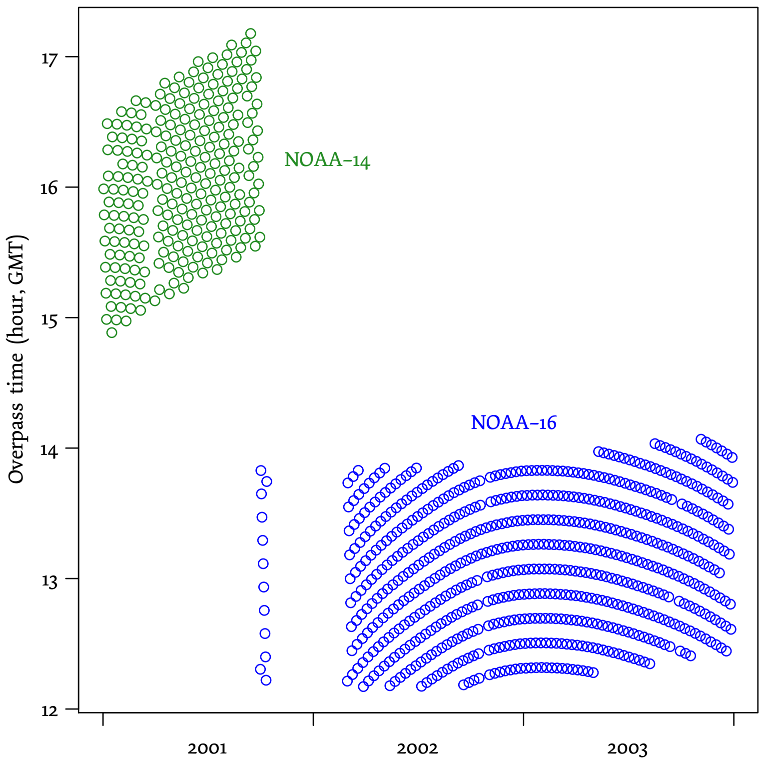

Fig. 3. Overpass times of the NOAA AVHRR platforms utilized for the daily LST maps at the centre of the Elbe River basin. Local solar time is about UTC + 50 min. The switch from NOAA-14 to NOAA-16 clearly shifted the bandwidth of scan times from late afternoon towards noon. Calculated from satellite equator crossing data available via URL http://www.noaasis.noaa.gov/NOAASIS/ml/navigation.html (last access: May 2012).

HESSD
10, 1127–1183, 2013

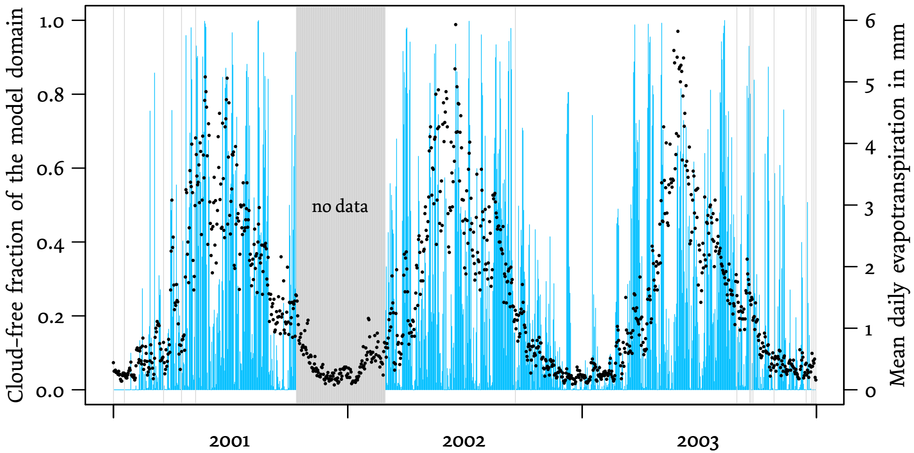

Fig. 4. Daily blue-sky fractions (lightblue, left hand y-axis) and average evapotranspiration rates (black dots, right hand y-axis) of the modelled part of the Elbe River basin. Cloud coverage was calculated from the available LST maps (grey colour indicates data gaps), and ET_a values were obtained from the globally pre-calibrated SWIM model.

HESSD
10, 1127–1183, 2013

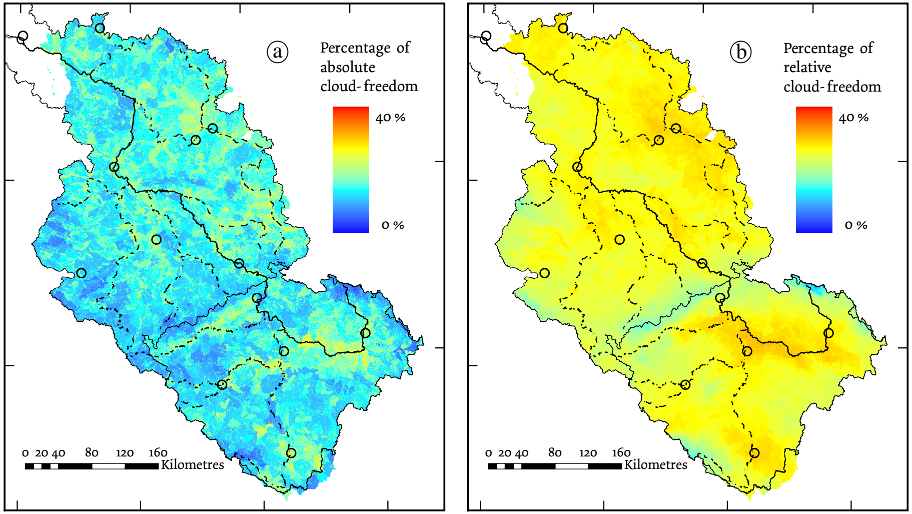

Fig. 5. Percentages of cloud-freedom in hydrotopes. **(a)** Absolute cloud-freedom: hydrotopes are coloured according to the share of scans in which they were entirely cloud-free, i.e. none of their raster cells were cloud-contaminated. **(b)** Relative cloud-freedom: mean fraction of cloud-free raster cells within the hydrotope, average of all scans. A legend to the orientation features is displayed in Fig. 6.

HESSD
10, 1127–1183, 2013

Three perceptions of the evapotranspiration landscape

T. Conradt et al.

Title Page
Abstract Introduction
Conclusions References
Tables Figures
◀◀ ▶▶
◀ ▶
Back Close
Full Screen / Esc
Printer-friendly Version
Interactive Discussion

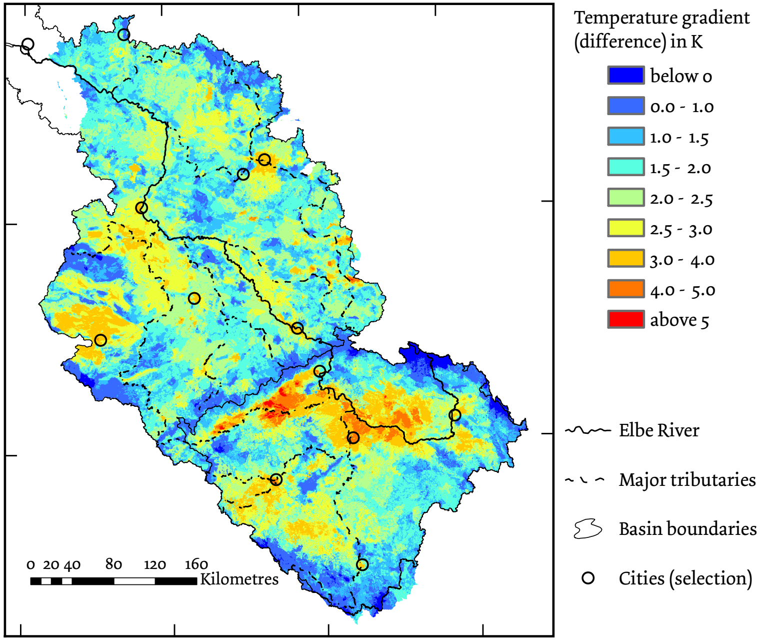

Fig. 6. Average temperature gradients: difference in K between surface and 2 m air temperatures. The originally observed differences between remotely sensed and ground measured temperature data have been corrected for cloud cover frequencies by Eq. (26).

HESSD
10, 1127–1183, 2013

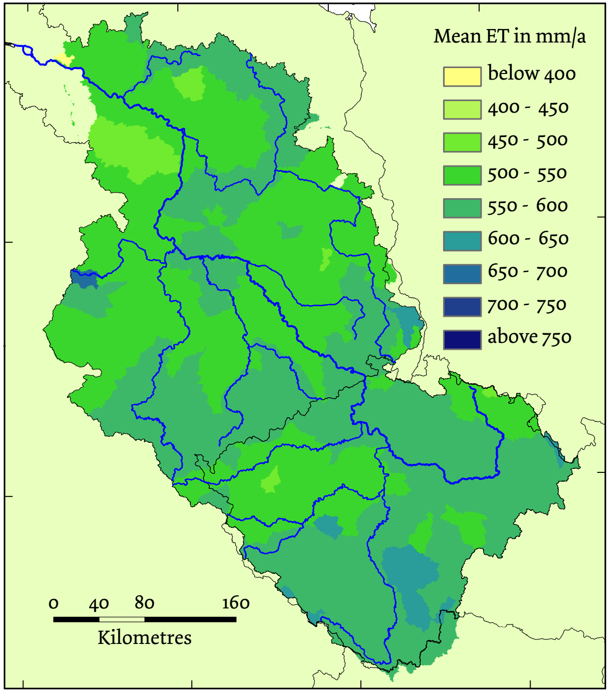

Fig. 7. Evapotranspiration patterns in the Elbe River basin according to SWIM. Average values for 133 sub-basins for the years 2001–2003.

HESSD
10, 1127–1183, 2013

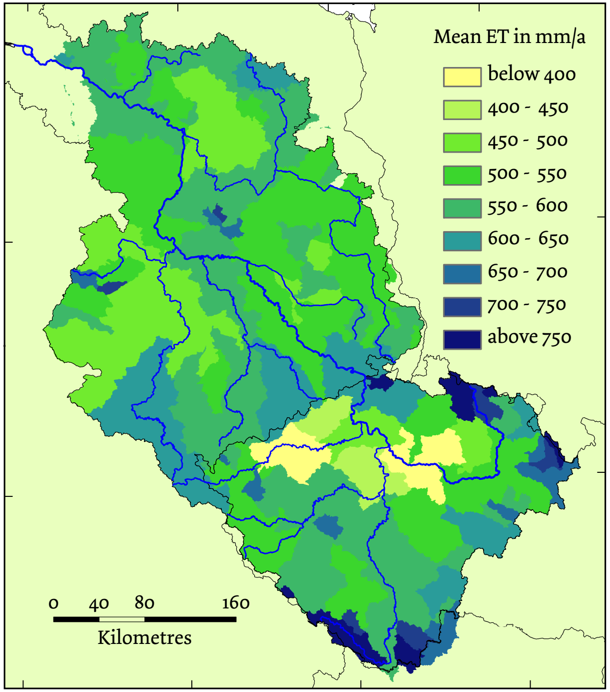

Fig. 8. Evapotranspiration patterns in the Elbe River basin according to remote sensing. Average values for 133 sub-basins for the years 2001–2003.

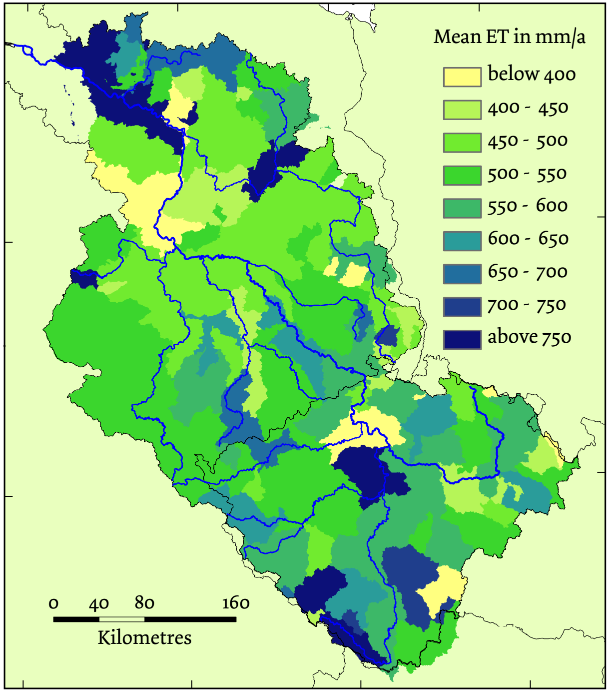

Fig. 9. Evapotranspiration patterns in the Elbe River basin according to the water balance. Average values for 133 sub-basins for the years 2001–2003.

HESSD
10, 1127–1183, 2013

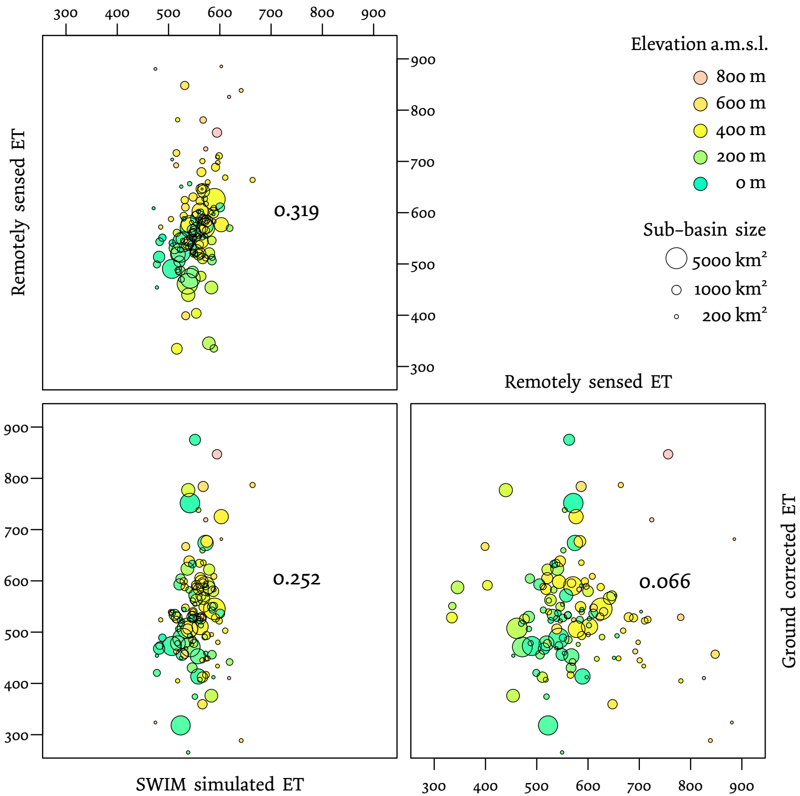

Fig. 10. Correlations between remotely sensed, SWIM simulated, and ground corrected evapotranspiration in $mm\,a^{-1}$.

HESSD
10, 1127–1183, 2013

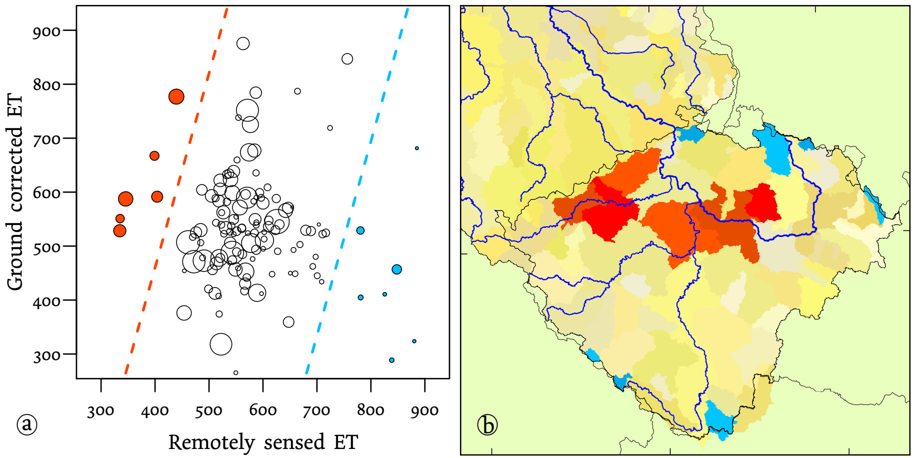

Fig. 11. Outlier clusters of sub-basins with strongly deviating remotely sensed and ground corrected ET. **(a)** Graphical separation of the clusters from the correlation plot, cf. the lower-right panel of Fig. 10. **(b)** Map cut-out with the respective sub-basins highlighted by their cluster colours.

HESSD
10, 1127–1183, 2013

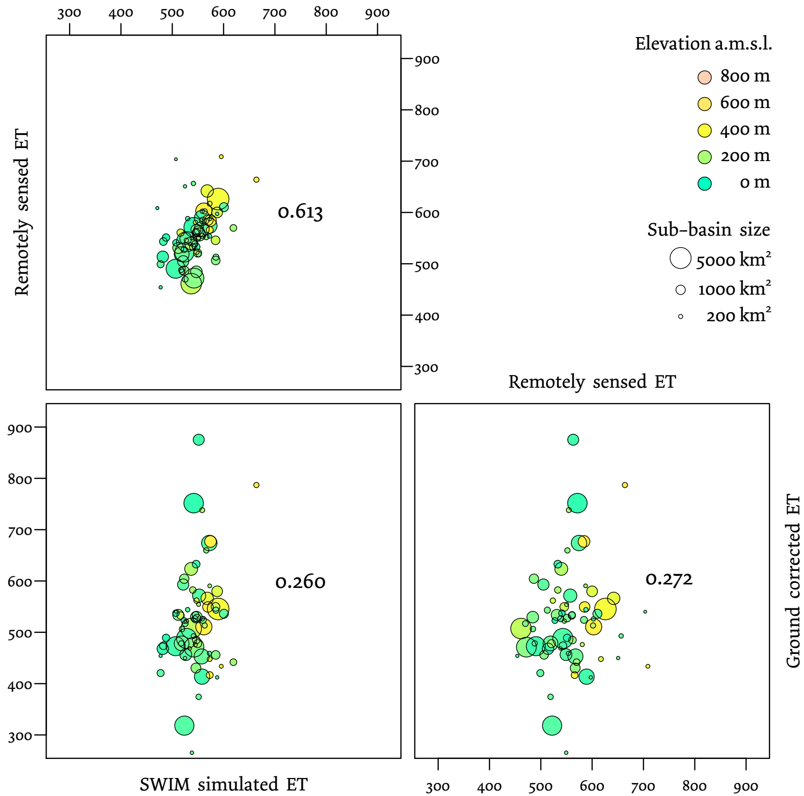

Fig. 12. Correlations between remotely sensed, SWIM simulated, and ground corrected evapotranspiration in $mm\,a^{-1}$ for the 72 sub-basins in the German part of the Elbe River basin.

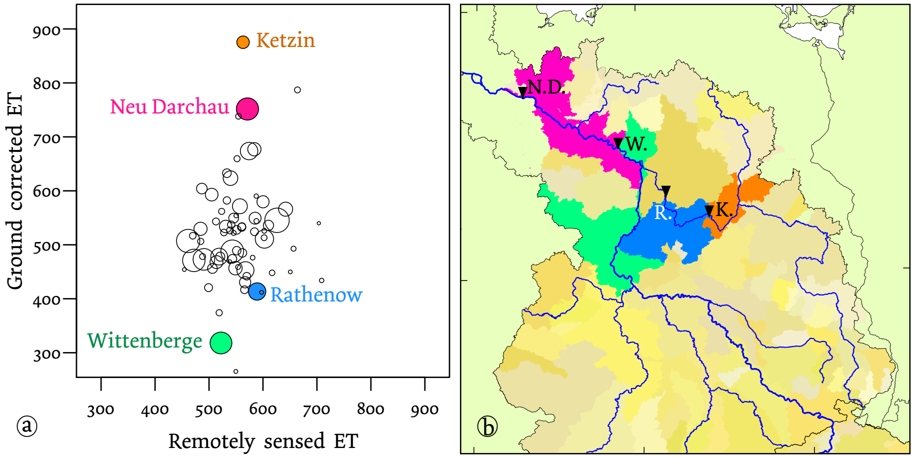

Fig. 13. Extreme differences between ground corrected ET from neighbouring sub-basins. The sub-basin areas in the dotty plot **(a)** are named according to their outlet gauges drawn in the map cut-out **(b)** as black triangles.

HESSD
10, 1127–1183, 2013

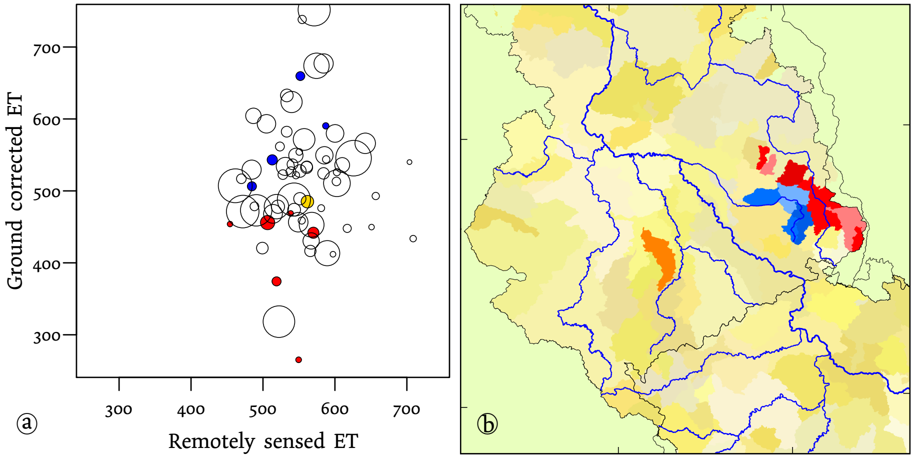

Fig. 14. Impacts of open cast mining on ground based ET corrections. Red: sub-basins along the Spree River with maximum ground water pumping in the 1980s. Blue: Schwarze Elster River sub-basins with less pronounced peak before 1970. Yellow/Orange: Pleiße River sub-basin covering an open cast mining area near Leipzig.

HESSD
10, 1127–1183, 2013